Inorganic Chemistry
Article
pubs.acs.org/IC

N-Heterocyclic Carbenes: Versatile Second Cyclometalated Ligands for Neutral Iridium(III) Heteroleptic Complexes

Tian-Yi Li,[†] Xiao Liang,[†] Liang Zhou,[‡] Chen Wu,[†] Song Zhang,[†] Xuan Liu,[†] Guang-Zhao Lu,[†] Li-Sha Xue,[†] You-Xuan Zheng,[*,†] and Jing-Lin Zuo[†]

[†]State Key Laboratory of Coordination Chemistry, Collaborative Innovation Center of Advanced Microstructures, Center for Molecular Organic Chemistry, School of Chemistry and Chemical Engineering, Nanjing University, Nanjing 210093, P. R. China

[‡]State Key Laboratory of Rare Earth Resource Utilization, Changchun Institute of Applied Chemistry, Chinese Academy of Sciences, Changchun, 130022, P. R. China

S *Supporting Information*

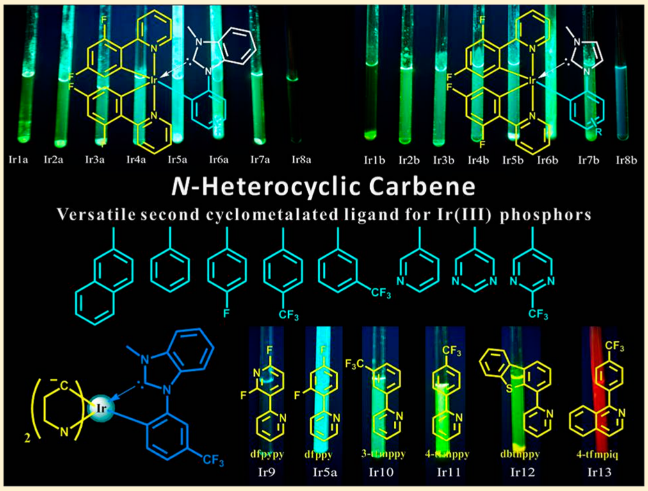

ABSTRACT: With 2-(2,4-difluorophenyl)pyridine (dfppy) as the first cyclometalated ligand and different monoanionic N-heterocyclic carbenes (NHCs) as the second cyclometalated ligands, 16 blue or greenish-blue neutral iridium(III) phosphorescent complexes, $(dfppy)_2Ir(NHC)$, were synthesized efficiently. The obtained Ir(III) complexes display typical phosphorescence of 455−485 nm with quantum yields up to 0.73. By modifying the phenyl moiety in the NHCs with electron-withdrawing substituents (e.g., −F or $-CF_3$) or replacing it with N-heteroaromatic rings (pyridine or pyrimidine), the HOMO−LUMO gaps are broadened, and the emissions shift to the more blue region accordingly. Furthermore, to extend the application scope of NHCs as the second cyclometalated ligands, five other Ir(III) complexes from blue to red were synthesized with different first cyclometalated ligands. Finally, the organic light-emitting diodes using one blue emitter exhibit a maximum current efficiency of 37.83 cd A^{-1}, an external quantum efficiency of 10.3%, and a maximum luminance of 8709 cd m^{-2}. Our results demonstrate that NHCs as the second cyclometalated ligands are good candidates for the achievement of efficient phosphorescent Ir(III) complexes and corresponding devices.

1. INTRODUCTION

Phosphorescent iridium(III) complexes are the favorable choices for organic light-emitting diodes (OLEDs) due to the high efficiency and stability.[1] With active design of ligands, phosphorescent Ir(III) complexes could exhibit a wide emission range from near-ultraviolet to red.[2] Recently, many high-performance single-color and white devices employing Ir(III) phosphors as emissive dopants have been reported.[3] However, the research on blue Ir(III) complexes is still vital because the devices with such emitters seldom show satisfying performances owing to the inherent contradiction between emission energy and photoluminescent quantum yield (PLQY).

From greenish-blue to deep blue, the seeking for blue materials is continuous and tough. Since the frontier molecular orbitals (FMOs), especially the highest occupied molecular orbital (HOMO) and the lowest unoccupied molecular orbital (LUMO), are crucial for the photophysical properties,[4] some popular strategies aiming to broaden the HOMO−LUMO gap are adopted to tune the emission to blue. To lower the HOMO energy of Ir(III) complexes, attaching the electron withdrawing moieties to the cyclometalated phenyl ring or replacing the phenyl ring with pyridine was effectual. According to the structure−property relationship,[4] Yang and co-workers developed blue Ir(III) complexes with fluorinated 1,3,4-oxadiazole derivatives as cyclometalated ligands.[5] Kang and co-workers reported a blue homoleptic complex $Ir(dfpypy)_3$ containing fluorine-substituted bipyridine ligand of 2′,6′-difluoro-2,3′-bipyridine.[6] Another strategy is to increase the LUMO energies by introducing the electron-donating groups into the pyridine ring. Wu and co-workers introduced electron-donating methoxy groups into the pyridine ring and achieve emission at 452 nm.[7] Using bipyridine ligand with methyl substitute, Kido and co-workers reported a pure blue emitter and the relevant devices, whose emission peak is at 454 nm with high power efficiency (30 lm W^{1-}) and external quantum efficiency (17%).[8] Replacement of pyridyl fragment in phenylpyridine ligands with other N-heterocyclic moieties, such as pyrazole, triazole, imidazole, have also been proved an efficient way to achieve blue emitters, since the LUMO energy levels are high

Received: August 13, 2014
Published: December 11, 2014

dx.doi.org/10.1021/ic501949h | *Inorg. Chem.* 2015, 54, 161−173

Scheme 1. Chemical Structures and Synthetic Routes of the Ligands and Complexes

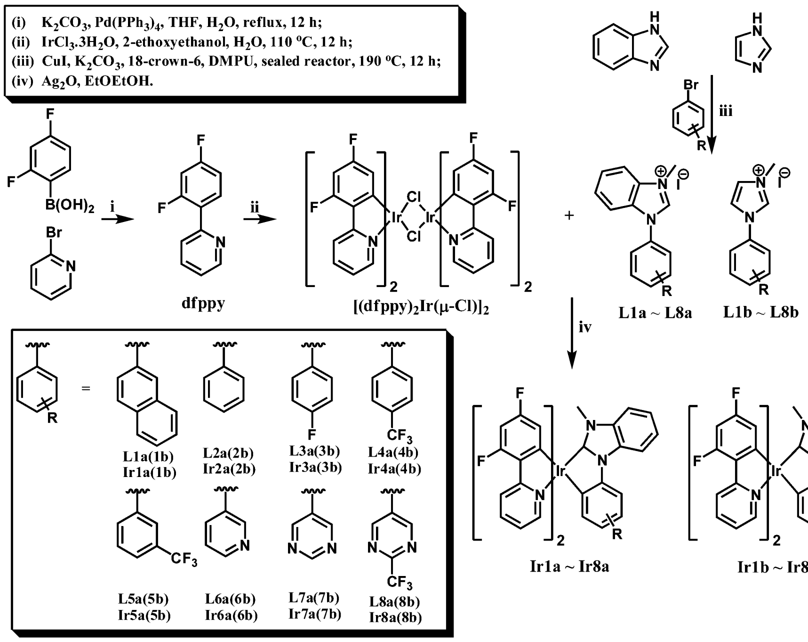

enough for blue emission in these materials.[9] De Cola and co-workers synthesized a series blue emitters with bipyridine main ligand and pyridyl−azole ancillary ligands. They display efficient genuine blue phosphorescence at ∼440 nm at room temperature with high quantum yield.[10] As reported by our group and others, although most ancillary ligands do not make a contribution to the lowest excited state directly, ancillary ligands with strong fields can help to increase the HOMO−LUMO energy gap and improve the device performances.[11] For example, iridium(III)bis(4,6-difluorophenyl-pyridinato)-picolinate (FIrpic)[12] and iridium(III)bis(4,6-difluorophenylpyridinato)tetrakis(1-pyrazolyl)borate (FIr6)[13] are efficient blue emitters due to their distinctive ancillary ligands.

With the σ-donating *N*-heterocyclic carbene ligands (NHCs), Ir(III) complexes with high triplet energy gaps can be used as blue emitters for OLEDs and electrochemical cells. Thompson and Forrest first reported the facial and meridional isomers *fac*/*mer*-Ir(pmb)$_3$ and *fac*/*mer*-Ir(pmi)$_3$ (pmb = 1-phenyl-3-methylbenzimidazole, pmi = 1-phenyl-3-methyl imidazole) exhibiting luminescence at ca. 380 nm.[14] Chi and co-workers reported the (dfbmb)$_2$Ir(fptz) (dfbmb = 1-(2,4-difluorobenzyl)-3-methylbenzimidazolium, fptz = 2-(3-(trifluoromethyl)-1*H*-1,2,4-triazol-5-yl)pyridine) complex with a pyridyl triazole ancillary ligand showing emission at 458 nm with a high quantum yield of 0.73.[15] Cheng and co-workers focused on neutral bis-carbene Ir(III) complexes, which covered a wide range of emission color from red to blue by changing the ancillary ligands.[16] Recently, Baranoff and co-workers successfully synthesized charged iridium complexes presenting fine-tunable emissions from near-UV to red with different cyclometalated ligands and found that the NHCs show a subsidiary tunable effect on the emission color.[17]

However, because of the difficulty of synthesis, in the past decade only several neutral carbene-based Ir(III) complexes have been reported, and few emitters showed interesting device performances. The direct synthetic route for Ir(NHC)$_3$ starting from carbene iodized salt precursors and IrCl$_3$·3H$_2$O resulted in a lower yield compared with the moderately high yield of phenylpyridine derivatives. The use of a dimer precursor [Ir(*μ*-Cl)(COD)$_2$]$_2$ (COD = 1,5-cyclooctadiene) was reported with high yields for the synthesis of some Ir(NHC)$_3$ complexes,[18] but the mixed *fac*/*mer*-Ir(NHC)$_3$ products with similar polarity hindered the further development.

In this study, with *N*-heteroleptic carbenes as the second cyclometalated ligands, a series of new type of (C^N)$_2$Ir(NHC) phosphors were synthesized efficiently. First, using dfppy (2-(2,4-difluorophenyl)pyridine) as the first cyclometalated ligand, 16 blue or greenish-blue complexes were obtained in good yields (Scheme 1). Considering that the NHCs have noticeable contributions to the HOMOs of the complexes, the NHCs were modified with phenyl, naphthalene, electron-withdrawing substituents, and *N*-heteroaromatic rings to investigate the relationship between the ligand structures and the photophysical properties. Second, by changing the first cyclometalated ligands, another five Ir(III) complexes from blue to red were synthesized. Finally, the OLEDs constructed with one blue emitter of them show interesting performances. Hence, we found a much easier and efficient method to introduce precious NHC ligands into neutral iridium phosphors, and our results demonstrate that the (C^N)$_2$Ir(NHC) configuration is a versatile and promising structure for interesting neutral phosphorescent Ir(III) complexes.

2. EXPERIMENTAL SECTION

General Information. An electrospray ionization (ESI) mass spectrometer (LCQ fleet, Thermo Fisher Scientific) was used to record mass spectra (MS) for the carbene ligands. High-resolution (HR) mass spectra (Agilent 6540 UHD Accurate-Mass Q-TOF LC/MS) were recorded for the complexes. ^{1}H NMR spectra were measured on a Bruker AM 500 spectrometer. UV−visible absorption and photoluminescence spectra were obtained using a Shimadzu UV-3100 and a Hitachi F-4600 spectrophotometer, respectively. The phosphorescence quantum yields were determined in nitrogen-deaerated CH$_2$Cl$_2$ solutions at 298 K against *fac*-Ir(ppy)$_3$ as a reference (Φ_P = 0.40).[19] The decay lifetimes were determined on an Edinburgh Instruments FLS-920 fluorescence spectrometer in degassed CH$_2$Cl$_2$ solutions at room temperature. A conventional three-electrode configuration, consisting of a polished Pt plate working electrode, a Pt wire counter electrode, and a reference electrode of Ag/$AgNO_3$ (0.1 M) in MeCN, was used to record cyclic voltammetry data in nitrogen-deaerated CH_3CN solution with 0.1 M $[Bu_4N]ClO_4$ as the supporting electrolyte and ferrocene as internal standard at a scan rate of 50 mV s^{-1}. The HOMO and LUMO energy levels were calculated using the equation HOMO (eV) = $E_{ox} - E_{Fc/Fc+} + 4.8$ and LUMO (eV) = $E_{red} - E_{Fc/Fc+} + 4.8$.

X-ray Crystallography. The crystallographic data were collected on a Siemens SMART CCD diffractometer (Bruker Daltonic Inc.) at room temperature using graphite-monochromated Mo Kα radiation (λ = 0.710 73 Å). The cell parameters were retrieved using SMART software and refined using SAINT on all observed reflections.[20] Absorption corrections were performed with SADABS supplied by Bruker.[21] All the calculations for the structure determination were carried out using the SHELXTL package.[22] Initial atomic positions were located by Patterson method using XS program, and the structures of the complexes were refined anisotropically by the least-squares method. Hydrogen atoms were fixed in calculated positions and refined as riding atoms with uniform U_{iso} values.

Theoretical Calculation. The density functional theory (DFT) and time-dependent DFT (TD-DFT) calculations were carried out with Gaussian 09 software package.[23] The geometries of the ground state (S_0) were fully optimized with the B3LYP exchange-correlation functional[24] using the LANL2DZ basis set[25] for iridium atom and the 6-31G** basis set[26] for the other atoms both in vacuum and in CH_2Cl_2 (C-PCM[27] solvent model). Vibrational frequency calculations were performed to validate that they are minima on potential energy surface. On the basis of the optimized S_0 molecular structures in solvent, TD-DFT calculation was performed, with M062x functional[28] and the same combination of basis sets, to determine the vertical transition characters and to simulate the UV–vis absorption spectra. Solvent effect was also considered by using C-PCM model. Frontier molecular orbitals were visualized using GaussView, and their quantified compositions in percentage on different parts were given by QMForge. GaussSum 2.2 was used to broaden the vertical transitions into simulated spectra, which were then compared with experimental data through Gaussian distribution with full width at half-maximum = 4000 cm^{-1}.

Fabrication of the OLEDs Device. Indium tin oxide (ITO) coated glass with a sheet resistance of 15 Ω sq^{-1} was used as the anode substrate. Successively, 1,1-bis(4-(di-*p*-tolylamino)phenyl)cyclohexane (TAPC, 40 nm), phosphorescent emitter doped in *N,N*′-dicarbazolyl-3,5-benzene host (mCP, 20 nm), 1,3,5-tri(*m*-pyrid-3-yl-phenyl)-benzene (TmPyPB,40 nm), LiF (1 nm), and Al (100 nm) were evaporated on the substrate. Current density–voltage–luminance (*J*–*V*–*L*) characteristics were measured by using a programmable Keithley source measurement unit (Keithley 2400 and Keithley 2000) with a silicon photodiode.

Synthesis and Characterization. All the synthesis experiments were carried out under nitrogen, and solvents were dried prior to use. All the μ-chloro-bridged dimer complexes used in this work, namely, $[(dfppy)_2Ir(\mu\text{-}Cl)]_2$, $[(4\text{-}tfmpiq)_2Ir(\mu\text{-}Cl)]_2$ (4-tfmpiq = 1-(4-(trifluoromethyl)phenyl)isoquinoline), $[(dbthppy)_2Ir(\mu\text{-}Cl)]_2$ (dbthppy = 2-(dibenzo[b,d]thiophen-4-yl)pyridine), $[(4\text{-}tfmppy)_2Ir(\mu\text{-}Cl)]_2$ (4-tfmppy = 2-(4-(trifluoromethyl)phenyl)pyridine), $[(3\text{-}tfmppy)_2Ir(\mu\text{-}Cl)]_2$ (3-tfmppy = 2-(3-(trifluoromethyl)phenyl)-pyridine), and $[(dfpypy)_2Ir(\mu\text{-}Cl)]_2$, were synthesized according to the reported methods by heating $IrCl_3{\cdot}3H_2O$ (1 equiv) and relevant cyclometalated ligand (2.2 equiv) in 2-ethoxyethanol and water (v/v = 3/1) at 110 °C.[29] Chemical structures and synthetic procedures of the Ir(III) complexes (**Ir1a-Ir8a**/**Ir1b-Ir8b** and **Ir9-Ir13**) are shown in Schemes 1 and 2.

General Synthesis of Carbene Precursors. A mixture of benzimidazole or imidazole (10.0 mmol), brominated benzene derivative (20.0 mmol), K_2CO_3 (20.0 mmol, 2.76 g), CuI (1.0 mmol, 0.19 g), 18-crown-6 (0.10 g), and DMPU (1,3-dimethyl-3,4,5,6-tetrahydro-2(1*H*)-pyrimidinone, 3 mL) was heated at 190 °C for 12 h in a sealed stainless reactor under nitrogen. The mixture was extracted with 200 mL of ethyl ether, and column chromatography (eluent = ethyl ether/hexane 1:1.5 v/v) gave the intermediate product. Then, the intermediate product and the same molar quantity of CH_3I were dissolved in 5 mL of tetrahydrofuran (THF) and stirred for 12 h. The NHC precursor as iodized salt was filtered and washed with THF giving the product as white powder.

Scheme 2[a]

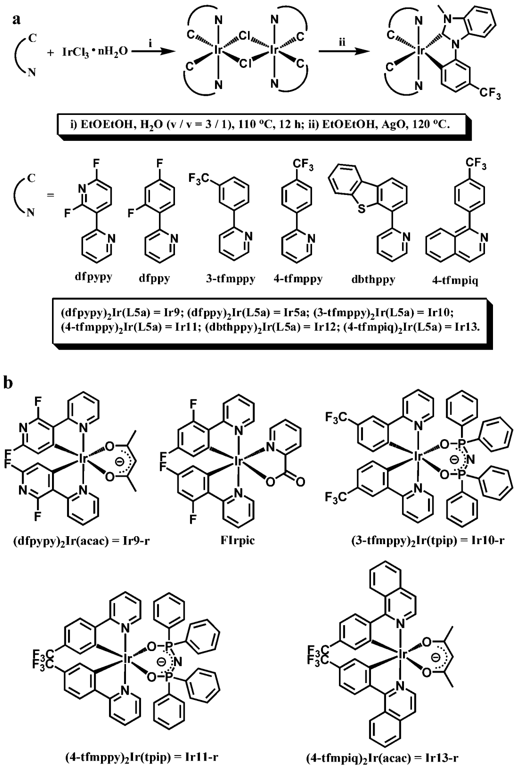

[a](a) The chemical structures and the synthetic routes of iridium complexes with different C^N cyclometalated ligands and **L5a** precursor. (b) The chemical structures of the reported iridium complexes cited in Table 2.

L1a. 2-Bromonaphthalene (4.12 g) and 1.18 g of benzimidazole gave 1.79 g of product (yield: 46%). ^1H NMR (500 MHz, deuterated dimethylsulfoxide (DMSO-d_6)) δ 10.29 (s, 1H), 8.48 (s, 1H), 8.34 (d, *J* = 8.7 Hz, 1H), 8.19 (dd, *J* = 18.9, 7.0 Hz, 3H), 7.95 (dd, *J* = 15.7, 5.0 Hz, 2H), 7.78 (ddd, *J* = 13.9, 12.1, 7.0 Hz, 4H), 4.24 (s, 3H). MS (ESI): calcd. for $[M - I]^+$ ($C_{18}H_{15}N_2^+$) *m*/*z* = 259.12, found 259.25.

L1b. 2-Bromonaphthalene (4.12 g) and 0.68 g of imidazole gave 2.17 g of product (yield: 65%). ^1H NMR (500 MHz, DMSO-d_6) δ 9.95 (s, 1H), 8.44 (s, 2H), 8.24 (d, *J* = 8.8 Hz, 1H), 8.06 (dd, *J* = 17.1, 10.4 Hz, 3H), 7.90 (d, *J* = 8.8 Hz, 1H), 7.68 (dq, *J* = 13.2, 6.5 Hz, 2H), 4.02 (s, 3H). MS (ESI): calcd. for $[M - I]^+$ ($C_{14}H_{13}N_2^+$) *m*/*z* = 209.11, found 209.17.

L2a. Bromobenzene (3.12 g) and 1.18 g of benzimidazole gave 1.65 g of product (yield: 49%). ^1H NMR (500 MHz, DMSO-d_6) δ 10.15 (s, 1H), 8.17 (d, *J* = 8.3 Hz, 1H), 7.89–7.68 (m, 8H), 4.19 (s, 3H). MS (ESI): calcd. for $[M - I]^+$ ($C_{14}H_{13}N_2^+$) *m*/*z* = 209.11, found 209.25.

L2b. Bromobenzene (3.12 g) and 0.68 g of imidazole gave 1.37 g of product (yield: 48%). ^1H NMR (500 MHz, DMSO-d_6) δ 9.82 (s, 1H), 8.31 (s, 1H), 7.99 (s, 1H), 7.80 (d, *J* = 7.7 Hz, 2H), 7.67 (t, *J* = 7.8 Hz, 2H), 7.59 (t, *J* = 7.4 Hz, 1H), 3.98 (s, 3H). MS (ESI): calcd. for $[M - I]^+$ ($C_{10}H_{11}N_2^+$) *m*/*z* = 159.09, found 159.17.

L3a. 1-Bromo-4-fluorobenzene (3.48 g) and 1.18 g of benzimidazole gave 1.66 g of product (yield: 47%). ^1H NMR (500 MHz, DMSO-d_6) δ 10.14 (s, 1H), 8.17 (d, *J* = 8.1 Hz, 1H), 7.92 (dd, *J* = 8.2, 4.6 Hz, 2H), 7.77 (dt, *J* = 15.3, 8.0 Hz, 3H), 7.64 (t, *J* = 8.5 Hz, 2H), 4.19 (s, 3H). MS (ESI): calcd. for $[M - I]^+$ ($C_{14}H_{12}FN_2^+$) *m*/*z* = 227.10, found 227.25.

L3b. 1-Bromo-4-fluorobenzene (3.48 g) and 0.68 g of imidazole gave 1.47 g of product (yield: 48%). ^1H NMR (500 MHz, DMSO-d_6)

δ 9.74 (s, 1H), 8.26 (s, 1H), 7.96 (s, 1H), 7.85 (dd, J = 8.8, 4.5 Hz, 2H), 7.56 (t, J = 8.7 Hz, 2H), 3.96 (s, 3H). MS (ESI): calcd. for $[M - I]^+$ ($C_{10}H_{10}FN_2^+$) m/z = 177.08, found 177.17.

L4a. 1-Bromo-4-(trifluoromethyl)benzene (4.48 g) and 1.18 g of benzimidazole gave 2.13 g of product (yield: 53%). ^{1}H NMR (500 MHz, DMSO-d_6) δ 10.25 (s, 1H), 8.19 (d, J = 8.4 Hz, 3H), 8.11 (d, J = 8.3 Hz, 2H), 7.94 (d, J = 8.3 Hz, 1H), 7.80 (dt, J = 29.0, 7.5 Hz, 2H), 4.22 (s, 3H). MS (ESI): calcd. for $[M - I]^+$ ($C_{15}H_{12}F_3N_2^+$) m/z = 277.09, found 277.25.

L4b. 1-Bromo-4-(trifluoromethyl)benzene (4.48 g) and 0.68 g of imidazole gave 2.17 g of product (yield: 61%). ^{1}H NMR (500 MHz, DMSO-d_6) δ 9.93 (s, 1H), 8.40 (s, 1H), 8.15−7.98 (m, 5H), 3.99 (s, 3H). MS (ESI): calcd. for $[M - I]^+$ ($C_{11}H_{10}F_3N_2^+$) m/z = 227.08, found 227.17.

L5a. 1-Bromo-3-(trifluoromethyl)benzene (4.48 g) and 1.18 g of benzimidazole gave 1.83 g of product (yield: 45%). ^{1}H NMR (500 MHz, DMSO-d_6) δ 10.23 (s, 1H), 8.29 (s, 1H), 8.20 (t, J = 9.1 Hz, 2H), 8.13 (d, J = 7.8 Hz, 1H), 8.03 (t, J = 7.9 Hz, 1H), 7.89 (d, J = 8.3 Hz, 1H), 7.86−7.79 (m, 1H), 7.79−7.71 (m, 1H), 4.21 (s, 3H). MS (ESI): calcd. for $[M - I]^+$ ($C_{15}H_{12}F_3N_2^+$) m/z = 277.09, found 277.25.

L5b. 1-Bromo-3-(trifluoromethyl)benzene (4.48 g) and 0.68 g of imidazole gave 1.60 g of product (yield: 45%). ^{1}H NMR (500 MHz, DMSO-d_6) δ 9.93 (s, 1H), 8.41 (d, J = 1.6 Hz, 1H), 8.25 (s, 1H), 8.14 (d, J = 7.9 Hz, 1H), 8.04−7.87 (m, 3H), 3.99 (s, 3H). MS (ESI): calcd. for $[M - I]^+$ ($C_{11}H_{10}F_3N_2^+$) m/z = 227.08, found 227.17.

L6a. 3-Bromopyridine (3.14 g) and 1.18 g of benzimidazole gave 1.25 g of product (yield: 37%). ^{1}H NMR (500 MHz, DMSO-d_6) δ 9.62 (s, 1H), 9.10 (d, J = 5.8 Hz, 1H), 9.00 (d, J = 8.3 Hz, 1H), 8.77 (s, 1H), 8.39 (t, J = 7.1 Hz, 1H), 7.93 (d, J = 8.0 Hz, 1H), 7.86 (d, J = 7.7 Hz, 1H), 7.49−7.40 (m, 2H), 4.49 (s, 3H). MS (ESI): calcd. for $[M - I]^+$ ($C_{13}H_{12}N_3^+$) m/z = 210.10, found 210.25.

L6b. 3-Bromopyridine (3.14 g) and 0.68 g of imidazole gave 1.38 g of product (yield: 48%). ^{1}H NMR (500 MHz, DMSO-d_6) δ 9.85 (s, 1H), 9.04 (d, J = 2.5 Hz, 1H), 8.96 (dd, J = 14.8, 7.2 Hz, 1H), 8.79 (d, J = 4.4 Hz, 1H), 8.35 (s, 1H), 8.25 (d, J = 8.2 Hz, 1H), 7.74 (dd, J = 8.2, 4.8 Hz, 1H), 3.99 (s, 3H). MS (ESI): calcd. for $[M - I]^+$ ($C_9H_{10}N_3^+$) m/z = 160.09, found 160.25.

L7a. 5-Bromopyrimidine (3.16 g) and 1.18 g of benzimidazole gave 1.45 g of product (yield: 43%). ^{1}H NMR (500 MHz, DMSO-d_6) δ 10.29 (s, 1H), 9.53 (s, 1H), 9.40 (s, 2H), 8.21 (d, J = 8.2 Hz, 1H), 8.01 (d, J = 8.2 Hz, 1H), 7.83 (t, J = 7.7 Hz, 1H), 7.77 (t, J = 7.7 Hz, 1H), 4.25 (s, 3H). MS (ESI): calcd. for [M − I]+ (C12H11N4$^+$) m/z = 211.10, found 211.25.

L7b. 5-Bromopyrimidine (3.16 g) and 0.68 g of imidazole gave 1.15 g of product (yield: 40%). ^{1}H NMR (500 MHz, DMSO-d_6) δ 9.90 (s, 1H), 9.40 (s, 1H), 9.31 (s, 2H), 8.38 (s, 1H), 8.04 (s, 1H), 4.01 (s, 3H). MS (ESI): calcd. for $[M - I]^+$ ($C_8H_9N_4^+$) m/z = 161.08, found 161.08.

L8a. 5-Bromo-2-(trifluoromethyl)pyrimidine (4.52 g) and 1.18 g of benzimidazole gave 1.59 g of product (yield: 39%). ^{1}H NMR (500 MHz, DMSO-d_6) δ 10.25 (s, 1H), 9.63 (s, 2H), 8.22 (d, J = 8.3 Hz, 1H), 8.11 (d, J = 8.2 Hz, 1H), 7.86−7.81 (m, 2H), 3.32 (s, 3H). MS (ESI): calcd. for $[M - I]^+$ ($C_{13}H_{10}F_3N_4^+$) m/z = 279.09, found 279.17.

L8b. 5-Bromo-2-(trifluoromethyl)pyrimidine (4.52 g) and 0.68 g of imidazole gave 2.06 g of product (yield: 58%). ^{1}H NMR (500 MHz, DMSO-d_6) δ 10.05 (s, 1H), 9.61 (s, 2H), 8.46 (s, 1H), 8.10 (s, 1H), 4.05 (s, 3H). MS (ESI): calcd. for $[M - I]^+$ ($C_9H_8F_3N_4^+$) m/z = 229.07, found 229.17.

General Synthesis of Iridium Complexes. A mixture of the μ-chloro-bridged dimer (0.4 mmol), the relative NHC precursors (0.88 mmol) and Ag_2O (0.70 mmol) was heated at 120 °C in 10 mL of 2-ethoxyethanol for 12 h protected from light. After the distillation of the solvent, the crude product was dissolved in CH_2Cl_2, and gray precipitate was filtered off. The filtrate was condensed and column chromatography (eluent = ethyl ether/hexane = 1.5:1 v/v) gave terminal product as yellow powder. All the target products were recrystallized from CH_2Cl_2 and MeOH.

Ir1a. $[(dfppy)_2Ir(\mu\text{-}Cl)]_2$ (0.49 g), 0.34 g **L1a**, and 0.16 g of silver(I) oxide gave 0.26 g of product (yield: 39%). ^{1}H NMR (500 MHz, DMSO-d_6) δ 8.71 (d, J = 8.0 Hz, 1H), 8.50 (s, 1H), 8.25 (d, J = 8.0 Hz, 1H), 8.18 (d, J = 8.2 Hz, 1H), 8.14 (d, J = 5.3 Hz, 1H), 8.02 (t, J = 7.1 Hz, 2H), 7.86−7.75 (m, 2H), 7.64 (d, J = 7.8 Hz, 1H), 7.53 (t, J = 7.6 Hz, 1H), 7.45 (t, J = 7.6 Hz, 1H), 7.30 (dd, J = 19.7, 7.4 Hz, 2H), 7.26−7.19 (m, 1H), 6.98 (s, 3H), 6.82−6.66 (m, 2H), 6.05 (d, J = 7.5 Hz, 1H), 5.66 (d, J = 8.1 Hz, 1H), 3.45 (s, 3H). HR electron impact (EI) MS Calcd: m/z 831.1717 for $[M + H]^+$ ($C_{40}H_{26}F_4IrN_4^+$), found: m/z 831.1714.

Ir1b. $[(dfppy)_2Ir(\mu\text{-}Cl)]_2$ (0.49 g), 0.27 g **L1b**, and 0.16 g of silver(I) oxide gave 0.25 g of product(yield: 41%). ^{1}H NMR (500 MHz, DMSO-d_6) δ 8.27 (d, J = 41.1 Hz, 3H), 8.16 (d, J = 7.7 Hz, 1H), 7.97 (t, J = 28.4 Hz, 3H), 7.88−7.75 (m, 2H), 7.67 (dd, J = 42.5, 24.4 Hz, 2H), 7.39−7.30 (m, 1H), 7.30−7.22 (m, 1H), 7.20 (d, J = 6.9 Hz, 1H), 7.04 (dd, J = 26.8, 18.9 Hz, 2H), 6.93 (s, 1H), 6.82−6.62 (m, 2H), 5.82−5.65 (m, 1H), 3.31 (s, 3H). HR EI-MS Calcd: m/z 781.1561 for $[M + H]^+$ ($C_{36}H_{24}F_4IrN_4^+$), found: m/z 781.1561.

Ir2a. $[(dfppy)_2Ir(\mu\text{-}Cl)]_2$ (0.49 g), 0.30 g **L2a**, and 0.16 g of silver(I) oxide gave 0.37 g of product (yield: 60%). ^{1}H NMR (500 MHz, DMSO-d_6) δ 8.40 (d, J = 7.7 Hz, 1H), 8.25 (dd, J = 15.9, 8.5 Hz, 2H), 8.08 (d, J = 5.3 Hz, 1H), 7.99 (dd, J = 17.2, 6.7 Hz, 2H), 7.84−7.78 (m, 1H), 7.58 (t, J = 11.6 Hz, 2H), 7.40 (dd, J = 17.5, 9.9 Hz, 2H), 7.10−6.96 (m, 3H), 6.78 (t, J = 6.7 Hz, 1H), 6.70 (t, J = 11.0 Hz, 2H), 6.62 (d, J = 7.3 Hz, 1H), 6.03 (d, J = 7.4 Hz, 1H), 5.59 (d, J = 7.9 Hz, 1H), 3.42 (s, 3H). HR EI-MS Calcd: m/z 781.1561 for $[M + H]^+$ ($C_{36}H_{24}F_4IrN_4^+$), found: m/z 781.1560.

Ir2b. $[(dfppy)_2Ir(\mu\text{-}Cl)]_2$ (0.49 g), 0.25 g **L2b**, and 0.16 g of silver(I) oxide gave 0.38 g of product (yield: 66%). ^{1}H NMR (500 MHz, DMSO-d_6) δ 8.21 (d, J = 8.4 Hz, 1H), 8.14 (d, J = 8.4 Hz, 1H), 8.04 (s, 1H), 8.00 (d, J = 5.6 Hz, 1H), 7.94 (d, J = 5.7 Hz, 1H), 7.81 (dt, J = 15.7, 7.7 Hz, 2H), 7.46 (d, J = 7.7 Hz, 1H), 7.26 (s, 1H), 7.08−7.01 (m, 2H), 6.91 (t, J = 7.5 Hz, 1H), 6.72 (t, J = 7.1 Hz, 1H), 6.69−6.60 (m, 2H), 6.54 (d, J = 7.0 Hz, 1H), 6.00 (d, J = 7.7 Hz, 1H), 5.64 (d, J = 8.3 Hz, 1H), 3.15 (s, 3H). HR EI-MS Calcd: m/z 731.1404 for $[M + H]^+$ ($C_{32}H_{22}F_4IrN_4^+$), found: m/z 731.1403.

Ir3a. $[(dfppy)_2Ir(\mu\text{-}Cl)]_2$ (0.49 g), 0.31 g **L3a**, and 0.16 g of silver(I) oxide gave 0.36 g of product (yield: 56%). ^{1}H NMR (500 MHz, DMSO-d_6) δ 8.38 (d, J = 7.6 Hz, 1H), 8.32 (d, J = 7.9 Hz, 1H), 8.30−8.22 (m, 2H), 8.22−8.17 (m, 1H), 8.09 (d, J = 5.5 Hz, 1H), 7.93 (d, J = 5.7 Hz, 1H), 7.85 (dd, J = 13.9, 7.1 Hz, 2H), 7.60 (d, J = 7.5 Hz, 2H), 7.47−7.37 (m, 2H), 7.06 (t, J = 6.4 Hz, 1H), 7.01 (t, J = 6.3 Hz, 1H), 6.78 (d, J = 11.2 Hz, 2H), 6.00 (d, J = 7.6 Hz, 1H), 5.60 (d, J = 8.0 Hz, 1H), 3.41 (s, 3H). HR EI-MS Calcd: m/z 799.1476 for $[M + H]^+$ ($C_{36}H_{23}F_5IrN_4^+$), found: m/z 799.1473.

Ir3b. $[(dfppy)_2Ir(\mu\text{-}Cl)]_2$ (0.49 g), 0.27 g **L3b**, and 0.16 g of silver(I) oxide gave 0.32 g of product (yield: 54%). ^{1}H NMR (500 MHz, DMSO-d_6) δ 8.22 (d, J = 8.0 Hz, 1H), 8.17 (d, J = 8.7 Hz, 1H), 8.04 (s, 1H), 7.94 (dd, J = 11.7, 5.6 Hz, 2H), 7.84 (dd, J = 18.3, 8.0 Hz, 2H), 7.52 (dd, J = 6.8, 4.4 Hz, 1H), 7.27 (s, 1H), 7.08 (t, J = 5.7 Hz, 2H), 6.74−6.61 (m, 3H), 6.15 (d, J = 8.7 Hz, 1H), 5.98 (d, J = 7.7 Hz, 1H), 5.64 (d, J = 8.2 Hz, 1H), 3.14 (s, 3H). HR EI-MS Calcd: m/z 749.1310 for $[M + H]^+$ ($C_{32}H_{21}F_5IrN_4^+$), found: m/z 749.1309.

Ir4a. $[(dfppy)_2Ir(\mu\text{-}Cl)]_2$ (0.49 g), 0.35 g **L4a**, and 0.16 g of silver(I) oxide gave 0.40 g of product (yield: 58%). ^{1}H NMR (500 MHz, DMSO-d_6) δ 8.44 (d, J = 7.8 Hz, 1H), 8.26 (d, J = 8.5 Hz, 1H), 8.19 (d, J = 8.0 Hz, 2H), 8.11 (d, J = 5.5 Hz, 1H), 7.91−7.81 (m, 3H), 7.63 (d, J = 7.6 Hz, 1H), 7.53−7.40 (m, 2H), 7.35 (d, J = 8.0 Hz, 1H), 7.07 (t, J = 6.2 Hz, 1H), 7.01 (t, J = 6.3 Hz, 1H), 6.85 (s, 1H), 6.75 (dd, J = 24.8, 13.0 Hz, 2H), 5.99 (d, J = 7.5 Hz, 1H), 5.60 (d, J = 8.0 Hz, 1H), 3.44 (s, 3H). HR EI-MS Calcd: m/z 849.1435 for $[M + H]^+$ ($C_{37}H_{23}F_7IrN_4^+$), found: m/z 849.1435.

Ir4b. $[(dfppy)_2Ir(\mu\text{-}Cl)]_2$ (0.49 g), 0.31 g **L4b**, and 0.16 g of silver(I) oxide gave 0.33 g of product (yield: 52%). ^{1}H NMR (500 MHz, DMSO-d_6) δ 8.23 (d, J = 8.1 Hz, 1H), 8.17 (s, 2H), 7.94 (d, J = 5.9 Hz, 1H), 7.90−7.80 (m, 3H), 7.67 (d, J = 8.2 Hz, 1H), 7.34 (s, 1H), 7.26 (d, J = 8.0 Hz, 1H), 7.08 (q, J = 6.4 Hz, 2H), 6.79 (s, 1H), 6.75−6.62 (m, 2H), 5.96 (d, J = 7.7 Hz, 1H), 5.65 (d, J = 8.1 Hz, 1H), 3.17 (s, 3H). HR EI-MS Calcd: m/z 799.1278 for $[M + H]^+$ ($C_{33}H_{21}F_7IrN_4^+$), found: m/z 799.1278.

Ir5a. $[(dfppy)_2Ir(\mu\text{-}Cl)]_2$ (0.49 g), 0.35 g **L5a**, and 0.16 g of silver(I) oxide gave 0.46 g of product (yield: 67%). ^{1}H NMR (500 MHz, DMSO-d_6) δ 8.34 (d, J = 8.1 Hz, 1H), 8.25 (d, J = 8.1 Hz, 1H), 8.19 (d, *J* = 8.1 Hz, 1H), 8.09 (s, 2H), 7.85 (dd, *J* = 18.3, 5.5 Hz, 3H), 7.63 (d, *J* = 7.8 Hz, 1H), 7.50 (t, *J* = 7.5 Hz, 1H), 7.47−7.41 (m, 1H), 7.12 (d, *J* = 7.3 Hz, 1H), 7.06 (t, *J* = 5.6 Hz, 1H), 7.01 (d, *J* = 5.8 Hz, 1H), 6.84 (d, *J* = 7.2 Hz, 1H), 6.78−6.68 (m, 2H), 5.99 (d, *J* = 7.4 Hz, 1H), 5.59 (d, *J* = 7.7 Hz, 1H), 3.43 (s, 3H). HR EI-MS Calcd: *m/z* 849.1435 for $[M + H]^+$ ($C_{37}H_{23}F_7IrN_4^+$), found: *m/z* 849.1433.

Ir5b. $[(dfppy)_2Ir(\mu\text{-}Cl)]_2$ (0.49 g), 0.31 g **L5b**, and 0.16 g of silver(I) oxide gave 0.38 g of product (yield: 59%). ^{1}H NMR (500 MHz, DMSO-d_6) δ 8.28 (s, 1H), 8.23 (d, *J* = 8.6 Hz, 1H), 8.16 (d, *J* = 7.9 Hz, 1H), 7.92 (d, *J* = 5.6 Hz, 1H), 7.88 (d, *J* = 5.7 Hz, 1H), 7.84 (t, *J* = 11.8 Hz, 3H), 7.32 (s, 1H), 7.08 (dd, *J* = 12.7, 6.5 Hz, 2H), 7.04 (d, *J* = 7.5 Hz, 1H), 6.75 (d, *J* = 7.5 Hz, 1H), 6.68 (dd, *J* = 22.2, 11.5 Hz, 2H), 5.96 (d, *J* = 7.7 Hz, 1H), 5.64 (d, *J* = 8.2 Hz, 1H), 3.16 (s, 3H). HR EI-MS Calcd: *m/z* 799.1278 for $[M + H]^+$ ($C_{33}H_{21}F_7IrN_4^+$), found: *m/z* 799.1279.

Ir6a. $[(dfppy)_2Ir(\mu\text{-}Cl)]_2$ (0.49 g), 0.30 g of **L6a**, and 0.16 g of silver(I) oxide gave 0.34 g of product (yield: 55%). ^{1}H NMR (500 MHz, CDCl$_3$) δ 8.38−8.20 (m, 2H), 8.03 (dd, *J* = 15.5, 6.9 Hz, 1H), 7.91−7.53 (m, 6H), 7.37 (d, *J* = 13.4 Hz, 2H), 7.10−7.00 (m, 1H), 7.00−6.90 (m, 1H), 6.89−6.64 (m, 2H), 6.50−6.41 (m, 1H), 6.40−6.11 (m, 2H), 5.66 (dd, *J* = 47.9, 8.4 Hz, 1H), 2.80 (s, 3H). HR EI-MS Calcd: *m/z* 782.1513 for $[M + H]^+$ ($C_{35}H_{23}F_4IrN_5^+$), found: *m/z* 782.1507.

Ir6b. $[(dfppy)_2Ir(\mu\text{-}Cl)]_2$ (0.49 g), 0.25 g of **L6b**, and 0.16 g of silver(I) oxide gave 0.30 g of product (yield: 51%). ^{1}H NMR (500 MHz, CDCl$_3$) δ 8.27 (ddd, *J* = 31.9, 22.5, 7.7 Hz, 3H), 7.89−7.51 (m, 5H), 7.05 (d, *J* = 21.7 Hz, 1H), 6.85 (t, *J* = 34.7 Hz, 2H), 6.66 (d, *J* = 19.0 Hz, 1H), 6.53−6.23 (m, 3H), 5.84−5.51 (m, 2H), 3.20 (s, 3H). HR EI-MS Calcd: *m/z* 732.1357 for $[M + H]^+$ ($C_{31}H_{21}F_4IrN_5^+$), found: *m/z* 732.1355.

Ir7a. $[(dfppy)_2Ir(\mu\text{-}Cl)]_2$ (0.49 g), 0.29 g of **L7a**, and 0.16 g of silver(I) oxide gave 0.39 g of product (yield: 63%). ^{1}H NMR (500 MHz, DMSO-d_6) δ 8.40 (d, *J* = 7.8 Hz, 1H), 8.24 (d, *J* = 8.3 Hz, 1H), 8.17 (d, *J* = 8.6 Hz, 1H), 8.08 (d, *J* = 5.1 Hz, 1H), 8.00 (d, *J* = 8.0 Hz, 1H), 7.97 (d, *J* = 5.8 Hz, 1H), 7.83 (dd, *J* = 16.9, 8.7 Hz, 2H), 7.60 (d, *J* = 7.7 Hz, 1H), 7.46−7.37 (m, 2H), 6.99 (t, *J* = 6.1 Hz, 1H), 6.78 (t, *J* = 7.1 Hz, 1H), 6.75−6.66 (m, 2H), 6.61 (d, *J* = 7.1 Hz, 1H), 6.03 (d, *J* = 7.5 Hz, 1H), 5.59 (d, *J* = 8.2 Hz, 1H), 3.42 (s, 3H). HR EI-MS Calcd: *m/z* 783.1466 for $[M + H]^+$ ($C_{34}H_{22}F_4IrN_6^+$), found: *m/z* 783.1464.

Ir7b. $[(dfppy)_2Ir(\mu\text{-}Cl)]_2$ (0.49 g), 0.25 g of **L7b**, and 0.16 g of silver(I) oxide gave 0.45 g of product (yield: 76%). ^{1}H NMR (500 MHz, DMSO-d_6) δ 9.80 (s, 1H), 9.23 (d, *J* = 8.4 Hz, 1H), 9.15 (s, 1H), 8.32 (d, *J* = 4.9 Hz, 1H), 8.29−8.21 (m, 2H), 8.20−8.10 (m, 2H), 8.02 (d, *J* = 20.4 Hz, 2H), 7.51 (s, 1H), 7.38 (s, 1H), 6.76 (dd, *J* = 20.1, 10.1 Hz, 1H), 6.70−6.59 (m, 1H), 5.71 (d, *J* = 7.8 Hz, 1H), 5.46 (d, *J* = 7.6 Hz, 1H), 3.31 (s, 3H). HR EI-MS Calcd: *m/z* 733.1309 for $[M + H]^+$ ($C_{30}H_{20}F_4IrN_6^+$), found: *m/z* 733.1309.

Ir8a. $[(dfppy)_2Ir(\mu\text{-}Cl)]_2$ (0.49 g), 0.35 g of **L8a**, and 0.16 g of silver(I) oxide gave 0.32 g of product (yield: 47%). ^{1}H NMR (500 MHz, DMSO-d_6) δ 9.80 (d, *J* = 5.6 Hz, 1H), 9.58 (d, *J* = 5.5 Hz, 1H), 8.79 (s, 1H), 8.32 (d, *J* = 8.4 Hz, 1H), 8.27 (d, *J* = 8.3 Hz, 1H), 8.22 (t, *J* = 7.8 Hz, 1H), 8.14 (t, *J* = 7.7 Hz, 1H), 7.89 (d, *J* = 7.5 Hz, 1H), 7.85 (d, *J* = 7.8 Hz, 1H), 7.68 (t, *J* = 6.5 Hz, 1H), 7.58 (t, *J* = 6.5 Hz, 1H), 7.41 (m, *J* = 7.2 Hz, 2H), 6.85 (t, *J* = 10.8 Hz, 1H), 6.79 (t, *J* = 10.8 Hz, 1H), 5.75 (d, *J* = 8.2 Hz, 1H), 5.09 (d, *J* = 8.6 Hz, 1H), 3.32 (s, 3H). HR EI-MS Calcd: *m/z* 851.1340 for $[M + H]^+$ ($C_{35}H_{21}F_7IrN_6^+$), found: *m/z* 851.1332.

Ir8b. $[(dfppy)_2Ir(\mu\text{-}Cl)]_2$ (0.49 g), 0.31 g of **L8b**, and 0.16 g of silver(I) oxide gave 0.32 g of product (yield: 49%). ^{1}H NMR (500 MHz, DMSO-d_6) δ 8.76 (s, 1H), 8.30−8.23 (m, 2H), 8.16 (d, *J* = 8.2 Hz, 1H), 7.88 (dd, *J* = 18.9, 10.7 Hz, 3H), 7.77 (d, *J* = 4.8 Hz, 1H), 7.45 (s, 1H), 7.10 (dd, *J* = 13.2, 6.3 Hz, 2H), 6.71 (t, *J* = 10.2 Hz, 1H), 6.63 (t, *J* = 10.4 Hz, 1H), 5.90 (d, *J* = 6.0 Hz, 1H), 5.58 (d, *J* = 6.8 Hz, 1H), 3.21 (s, 3H). HR EI-MS Calcd: *m/z* 801.1183 for $[M + H]^+$ ($C_{31}H_{19}F_7IrN_6^+$), found: *m/z* 801.1184.

*$(dfpypy)_2Ir$(**L5a**) (**Ir9**).* $[(dfpypy)_2Ir(\mu\text{-}Cl)]_2$ (0.49 g), 0.35 g of **L5a**, and 0.16 g of silver(I) oxide gave 0.35 g of product (yield: 51%). ^{1}H NMR (500 MHz, DMSO-d_6) δ 8.38 (d, *J* = 8.1 Hz, 1H), 8.27 (d, *J* = 8.2 Hz, 1H), 8.19 (dd, *J* = 13.7, 7.1 Hz, 2H), 8.12 (s, 1H), 7.96 (dd, *J* = 18.4, 8.2 Hz, 2H), 7.90 (d, *J* = 5.7 Hz, 1H), 7.69 (d, *J* = 7.9 Hz, 1H), 7.52 (t, *J* = 7.7 Hz, 1H), 7.47 (t, *J* = 7.6 Hz, 1H), 7.17 (dd, *J* = 13.2, 6.6 Hz, 3H), 6.82 (d, *J* = 7.4 Hz, 1H), 6.04 (s, 1H), 5.62 (s, 1H), 3.47 (s, 3H). HR EI-MS Calcd: *m/z* 851.1340 for $[M + H]^+$ ($C_{35}H_{21}F_7IrN_6^+$), found: *m/z* 851.1339.

*$(3\text{-}tfmppy)_2Ir$(**L5a**) (**Ir10**).* $[(3\text{-}tfmppy)_2Ir(\mu\text{-}Cl)]_2$ (0.53 g), 0.35 g of **L5a**, and 0.16 g of silver(I) oxide gave 0.47 g of product (yield: 64%). ^{1}H NMR (500 MHz, DMSO-d_6) δ 8.40 (d, *J* = 7.7 Hz, 1H), 8.33 (d, *J* = 6.3 Hz, 2H), 8.21 (s, 1H), 8.14−8.05 (m, 3H), 8.00 (t, *J* = 8.7 Hz, 1H), 7.86−7.79 (m, 1H), 7.59 (dd, *J* = 16.5, 8.9 Hz, 2H), 7.43 (dd, *J* = 13.6, 6.5 Hz, 2H), 7.10 (dd, *J* = 21.3, 11.5 Hz, 3H), 7.05−6.99 (m, 2H), 6.98−6.91 (m, 1H), 6.82−6.71 (m, 1H), 6.34 (dd, *J* = 19.3, 7.6 Hz, 1H), 3.36 (s, 3H). HR EI-MS Calcd: *m/z* 913.1559 for $[M + H]^+$ ($C_{39}H_{25}F_9IrN_4^+$), found: *m/z* 913.1561.

*$(4\text{-}tfmppy)_2Ir$(**L5a**) (**Ir11**).* $[(4\text{-}tfmppy)_2Ir(\mu\text{-}Cl)]_2$ (0.53 g), 0.35 g of **L5a**, and 0.16 g of silver(I) oxide gave 0.49 g of product (yield: 67%).^{1}H NMR (500 MHz, DMSO-d_6) δ 8.33 (t, 2H), 8.27 (d, *J* = 8.1 Hz, 1H), 8.13 (dd, *J* = 13.9, 6.9 Hz, 2H), 8.09−8.02 (m, 2H), 7.92 (d, *J* = 5.8 Hz, 1H), 7.91−7.82 (m, 2H), 7.61 (d, *J* = 8.0 Hz, 1H), 7.49 (t, *J* = 7.7 Hz, 1H), 7.42 (t, *J* = 7.6 Hz, 1H), 7.22 (d, *J* = 7.8 Hz, 2H), 7.14 (t, *J* = 6.6 Hz, 1H), 7.08 (d, *J* = 6.9 Hz, 2H), 6.77 (d, *J* = 12.1 Hz, 2H), 6.38 (s, 1H), 3.34 (s, 3H). HR EI-MS Calcd: *m/z* 913.1559 for $[M + H]^+$ ($C_{39}H_{25}F_9IrN_4^+$), found: *m/z* 913.1555.

*(dbthppy)2Ir(**L5a**) (**Ir12**).* [(dbthppy)2Ir(μ-Cl)]2 (0.60 g), 0.35 g of **L5a**, and 0.16 g of silver(I) oxide gave 0.42 g of product (yield: 53%). ^{1}H NMR (500 MHz, DMSO-d_6) δ 8.43 (d, *J* = 8.2 Hz, 1H), 8.36 (t, *J* = 7.8 Hz, 2H), 8.31 (d, *J* = 5.7 Hz, 1H), 8.15 (d, *J* = 7.0 Hz, 2H), 8.11 (d, *J* = 6.2 Hz, 2H), 8.06 (d, *J* = 7.5 Hz, 2H), 8.00 (d, *J* = 8.5 Hz, 3H), 7.84 (d, *J* = 7.8 Hz, 2H), 7.57−7.51 (m, 2H), 7.47−7.39 (m, 6H), 7.12 (dt, *J* = 12.5, 6.6 Hz, 2H), 7.00 (t, *J* = 6.8 Hz, 1H), 6.82 (d, *J* = 7.4 Hz, 1H), 3.32 (s, 3H). HR EI-MS Calcd: *m/z* 989.1566 for $[M + H]^+$ ($C_{49}H_{31}F_3IrN_4S_2^+$), found: *m/z* 989.1562.

*$(4\text{-}tfmpiq)_2Ir$(**L5a**) (**Ir13**).* $[(4\text{-}tfmpiq)_2Ir(\mu\text{-}Cl)]_2$ (0.62 g), 0.35 g of **L5a**, and 0.16 g of silver(I) oxide gave 0.45 g of product as deep red powder (yield: 56%). ^{1}H NMR (500 MHz, CDCl$_3$) δ 8.95−8.86 (m, 2H), 8.32 (d, *J* = 8.3 Hz, 1H), 8.26 (d, *J* = 8.3 Hz, 1H), 8.11 (d, *J* = 8.3 Hz, 1H), 8.00 (t, *J* = 7.9 Hz, 1H), 7.83 (dd, *J* = 20.8, 7.1 Hz, 3H), 7.74 (dt, *J* = 12.8, 4.9 Hz, 4H), 7.42−7.36 (m, *J* = 11.6, 7.3 Hz, 3H), 7.31 (dt, *J* = 17.8, 8.9 Hz, 5H), 7.26−7.21 (m, 2H), 7.02 (dd, *J* = 11.8, 6.4 Hz, 2H), 3.47 (s, 3H). HR EI-MS Calcd: *m/z* 1035.1692 for $[M + Na]^+$ ($C_{47}H_{28}F_9IrN_4Na^+$), found: *m/z* 1035.1691.

3. RESULTS AND DISCUSSION

Molecular Design, Synthesis, and Chemical Characterization. The iodized carbene precursors were prepared by the modified Ullmann coupling reaction of benzimidazole or imidazole with the corresponding bromonaphthalene, bromobenzene, bromopyridine, or bromopyrimidine derivatives, followed by *N*-methylation with iodomethane. Then, the target Ir(III) complexes were synthesized by heating the mixture of Ir(III) μ-chloro-bridged dimer, NHC precursors, and Ag$_2$O in 2-ethoxyethanol. According to the previous reports,[15] during the process of the formation of Ir(III) complexes, 2 mol NHC precursors coordinate with 1 mol Ag(I) *in situ* forming the carbene coordination structures. Then, the silver carbene complexes were reacted directly with the μ-chloro-bridged dimers performing the transition of the carbene ligands to the iridium center. Also, the silver cation promoted the progress due to the formation of AgCl.

The results from DFT calculations suggest that the modification on the phenyl moiety of the NHCs makes a distinctive difference on the FMOs and photophysical properties of the complexes. On the basis of this theoretical guideline, electron-withdrawing moieties (−CF$_3$, −F) and *N*-heteroaromatic rings (pyridine, pyrimidine) are introduced into NHCs for larger HOMO−LUMO gap and emission hypsochromic shift. Meanwhile, the replacement of phenyl ring with more conjugated naphthalene ring is expected to gain a bathochromic shift. Here, 16 blue or greenish-blue iridium complexes $(dfppy)_2Ir$(**L1a**~**L8a**) (**Ir1a**~**Ir8a**) and $(dfppy)_2Ir$(**L1b**~**L8b**) (**Ir1b**~**Ir8b**) containing second cyclometalated NHC ligands were synthesized in good yields (39−76%). Furthermore, another five complexes (**Ir9**−**Ir13**) with different first cyclometalated ligands from blue to red were synthesized to confirm the extensive application of NHC as a second cyclometalated ligand and the corresponding effects on emission properties.

The synthesized Ir(III) complexes were characterized with ^{1}H NMR (Figure 1) and high-resolution mass spectroscopy (HR MS, ESI). As shown in Figure 1, single peaks (marked with asterisk at 10.29 ppm for **L1a** and at 10.25 ppm for **L4a**) with integral of one hydrogen in high field can be assigned to the pro-carbenic proton in the ^{1}H NMR spectra of the NHC precursors because of the electron-withdrawing effect of cation together with the shielding effect of the imidazole conjunction structure. After the complexes were formed, these signals disappeared. This further confirmed the formation of the carbene−Ir structures.

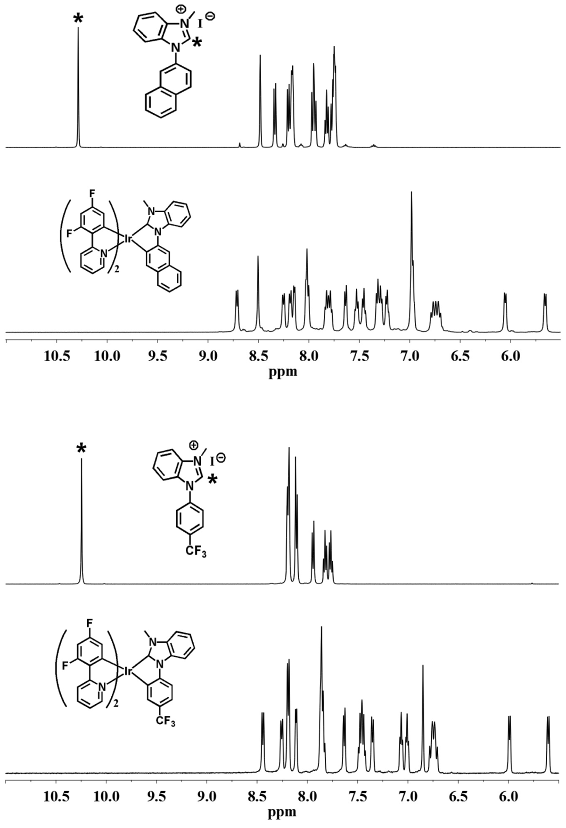

Figure 1. ^{1}H NMR spectra of **L1a**/**Ir1a** (top) and **L4a**/**Ir4a** (bottom).

The structures of the Ir(III) phosphors were further confirmed by the single-crystal X-ray diffraction analysis. Ten crystals (CCDC numbers: 986474−986483) were obtained either by solvent diffusion (MeOH into CH_2Cl_2 solutions for **Ir2a**, **Ir2b**, **Ir3a**, **Ir3b**, **Ir4a**, **Ir5a**, **Ir5b**, **Ir8b**, and **Ir9**) or by controlled sublimation (**Ir11**) under high vacuum atmosphere. The perspective diagrams of these complexes were depicted in Figure 2. The corresponding crystallographic data were collected in Supporting Information, Table S1, and the selected bond lengths and angles were listed in Supporting Information, Table S2. In the coordination sphere, the iridium center coordinates to two C^N ligands and one NHC ligand. The C^N ligands adopt a mutually eclipsed configuration, with the N atoms residing at the *trans* and *cis* locations for C atoms. All the coordination bonds are longer than 2.00 Å. The Ir−C1 bonds are in the range of 2.019 to 2.110 Å, and the Ir−C2 bonds are slightly longer than Ir−C1 bonds (except **Ir8b**), demonstrating a stable coordination via electrons donated by carbene C: atoms. As a result of the five-membered structure of imidazole ring, C1−Ir−C2 angles are all less than 90°, and some are even less than 80°. The N1−Ir−N2 angles are ~170°, presenting an obviously distorted octahedral geometry around the iridium center. These structural characteristics can also be found in other reported Ir(III) complexes with neutral NHCs.[30]

Electrochemistry and DFT/TD-DFT Calculation. The redox properties and HOMO/LUMOs of the emitters have impact on the charge transport ability and the OLED structure. To investigate the NHCs effect, cyclic voltammetry measurements were performed on **Ir1a-Ir8a** and **Ir1b-Ir8b**. The HOMO/LUMOs calculated with ferrocene as standard reference were listed in Supporting Information, Table S3. During the anodic scan in MeCN, each complex exhibits a

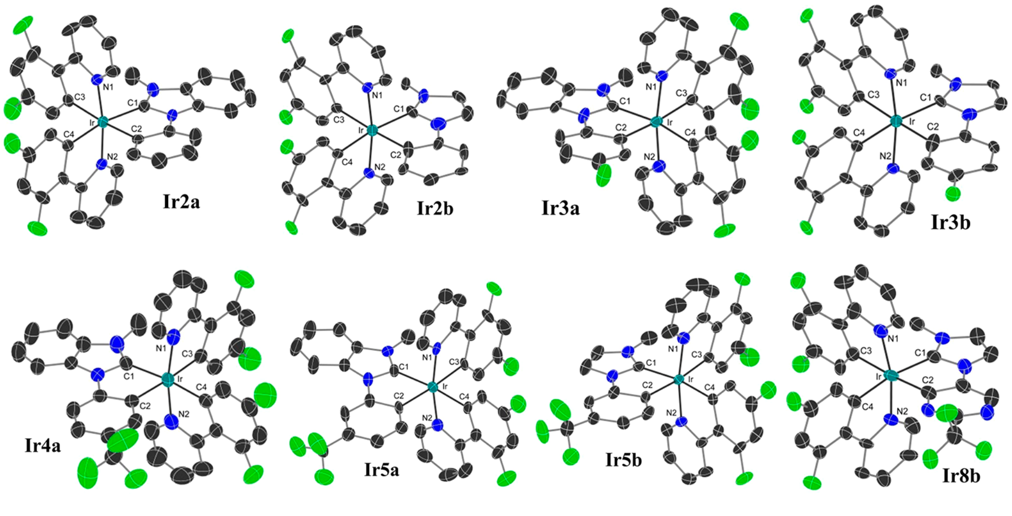

Figure 2. Perspective diagrams of X-ray crystal structures of studied complexes with dfppy ligand. (Thermal ellipsoids shown at 40% probability level; H atoms and solvent molecules are omitted for clarity.) Labels are added on the atoms bonded to the iridium center.

partial reversible process with strong oxidation peaks and unobvious reduction peaks, which could be assigned to metal-centered Ir(III)/Ir(IV) redox couple (Supporting Information, Figure S1). When the phenyl unit in carbene ligands was replaced, the oxidation and reduction potentials of Ir complexes were positive-shifted. This phenomenon was also observed in iridium complexes with ancillary ligands, which account for a relatively large proportion of the HOMOs.[11f] In the negative potential scan range, all the complexes show quasi-reversible redox peaks mainly due to the reduction of dfppy ligands. From Supporting Information, Table S3, it could be found that from **Ir1a** to **Ir5a** and from **Ir1b** to **Ir5b**, the substitution of electron-withdrawing substitutes caused a positive shift in E_{ox} at ~100 mV. Consequently, the HOMOs are stabilized, and the $\Delta E_{(HOMO-LUMO)}$ gaps ($E_{ox} - E_{red}$) are broadened, which agree with Barnard and Hogan's results.[31] Furthermore, when the phenyl rings are replaced by pyridine and pyrimidine rings, the HOMOs are further stabilized, and the $\Delta E_{(HOMO-LUMO)}$ gaps are much larger in **Ir6a**/**Ir6b**, **Ir7a**/**Ir7b**, and **Ir8a**/**Ir8b**. These results are well-consistent with the shifts of emission peaks of these complexes. Supported by the theoretical calculation results and also proved by the following photophysical properties measurements, our molecular design of the NHCs indeed can tune the emission of the iridium phosphors, which turns out to be a rational and useful design method. This trend is further reproduced by the following theoretical calculation results and is reflected in the variation of the emission spectra.

Information about the energy level and electronic structure of the FMOs was provided by the computational calculations. The results are helpful for the assignment of the electron transition characteristics and the discussion on the photophysical variations. Thus, the ground-state geometries of all the Ir(III) complexes were fully optimized using DFT method with B3LYP functional. The energies and the compositions of the FMOs are collected in Supporting Information, Table S4, and the contour plots of HOMOs and LUMOs are listed in Supporting Information, Figure S2. Furthermore, Figure 3 schematically illustrates the changing trend of these orbitals. TD-DFT calculations were based on the optimized ground-state structures and certain vertical transitions, which could reveal the nature of different UV–vis absorption bands that were selected in Supporting Information, Table S5.

From Supporting Information, Table S4, it can be found that the LUMOs have similar compositions and are located mainly on the two dfppy ligands (~93%). Therefore, the LUMOs are exactly the same. However, the HOMOs present a clear variation trend that is consistent with our molecular design. Since the π orbital energy of the naphthyl is higher-lying, the HOMOs of **Ir1a**/**Ir1b**, which have the largest contributions from the NHCs, are the highest ones. With the replacement of naphthyl by phenyl and with electron-withdrawing fluorine/trifluoromethyl-substituted phenyl, due to the stabilization effect, the HOMOs decrease to a certain extent in **Ir2a**/**Ir2b**–**Ir5a**/**Ir5b**. The following alternation of phenyl moiety to pyridyl and pyrimidyl moieties further minimizes the occupation ratios of NHCs in HOMOs, and the energy levels are lowered from **Ir6a**/**Ir6b** to **Ir8a**/**Ir8b**, gradually.

Photophysical Property. The absorption and emission spectra of all complexes measured at room temperature or 77 K in CH_2Cl_2 solution were given in Figures 4 and 5, and the photophysical data were summarized in Table 1. All the $(dfppy)_2Ir(NHC)$ complexes show broad and intense absorp-

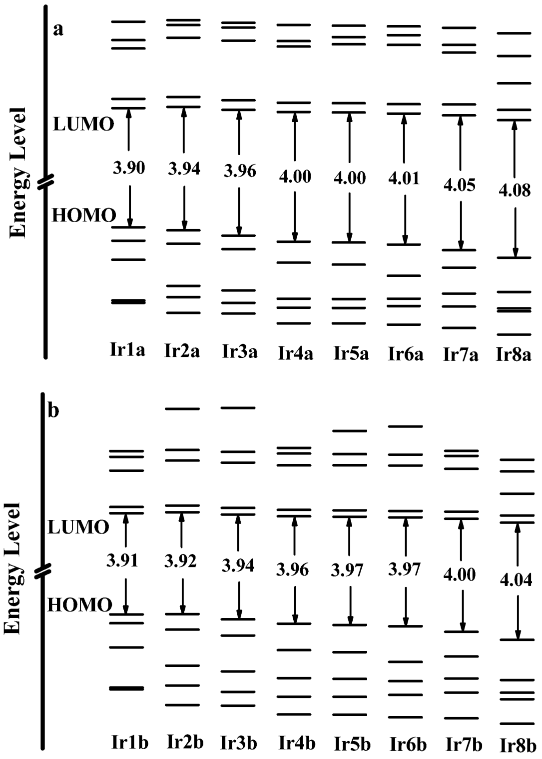

Figure 3. Schematic representations of the calculated FMOs of **Ir1a**–**Ir8a** (a) and **Ir1b**–**Ir8b** (b).

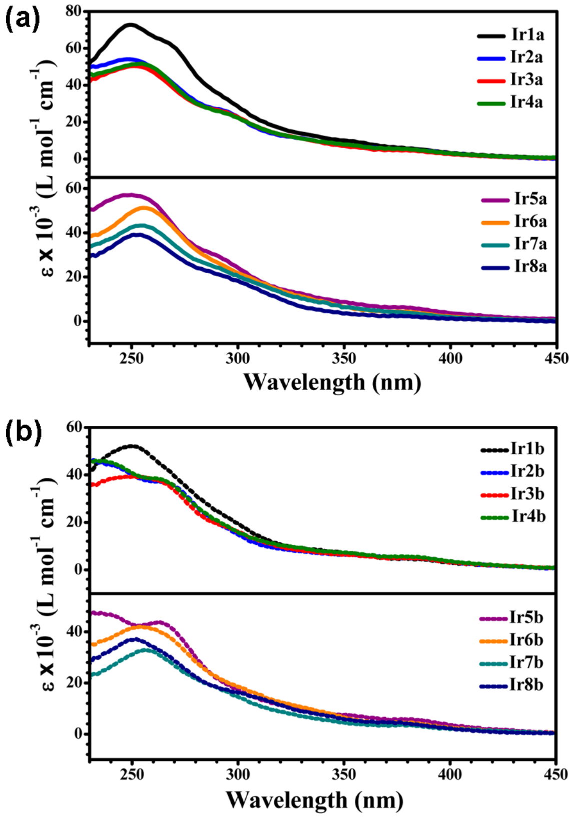

Figure 4. UV–vis absorption spectra of **Ir1a**–**Ir8a** (a) and **Ir1b**–**Ir8b** (b). All the spectra were measured in CH_2Cl_2 (5×10^{-6} M) at room temperature.

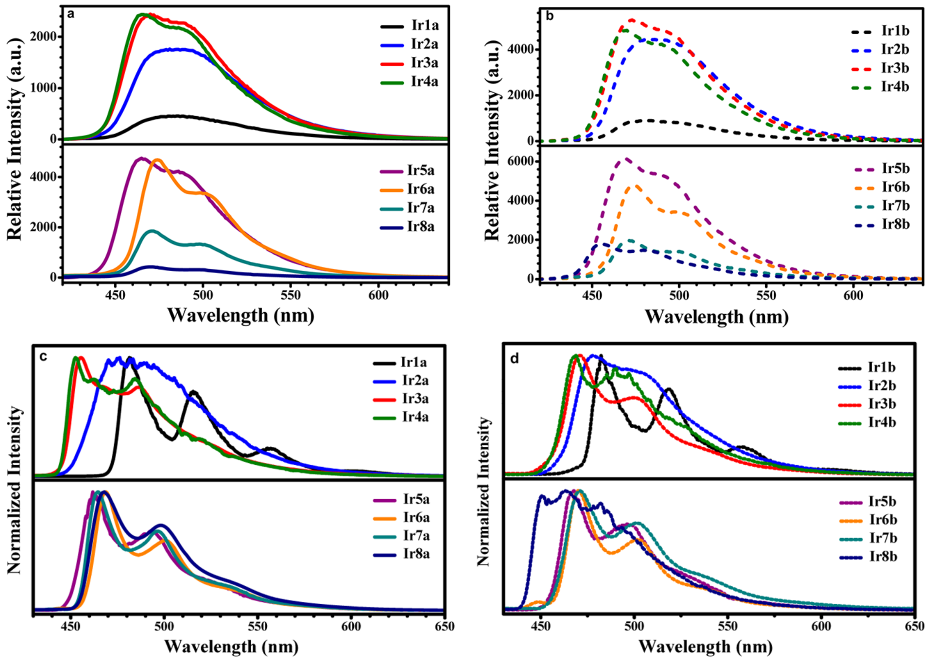

Figure 5. Emission spectra of **Ir1a**−**Ir8a** (a) and **Ir1b**−**Ir8b** (b) at room temperature. The normalized emission spectra of **Ir1a**−**Ir8a** (c) and **Ir1b**−**Ir8b** (d) at 77 K. All the samples are in the deaerated CH_2Cl_2 solutions (5×10^{-5} M).

Table 1. Photophysical Properties of Ir1a−Ir8a and Ir1b−Ir8b

	absorption at 298 K[a]	emission at 298 K[b]				emission at 77 K
		λ_{em} (nm)				
complex	λ_{abs} (ε) (nm ($\times 10^{-3}$ L mol^{-1} cm^{-1}))	CH_2Cl_2	MeCN	τ (μs)	Φ_{PL}[c]	λ_{max} (nm)
Ir1a	250 (72.7)	485	481	1.9	0.06	481, 515, 556
Ir1b	249 (52.1), 381 (4.7)	483	488	2.1	0.14	482, 519, 557
Ir2a	248 (54.1), 291 (27.1), 329 (11.4), 380 (5.2)	485	494	1.7	0.26	470, 475, 482
Ir2b	228 (48.0), 262 (37.3), 384 (5.0)	483	494	1.8	0.65	478, 503(sh)
Ir3a	251 (50.4), 293 (25.7), 379 (4.9)	470, 490(sh)	484	1.9	0.37	455, 486
Ir3b	250 (39.3), 381 (5.0)	473, 491(sh)	480	1.8	0.73	471, 500
Ir4a	255 (51.7), 290 (26.0), 375 (5.7)	465, 486(sh)	474	1.8	0.30	452, 462, 484
Ir4b	233 (46.2), 260 (38.7), 378 (5.7)	469, 487(sh)	477	1.9	0.57	469, 490
Ir5a	249 (57.2), 285 (31.8), 377 (6.4)	465, 485(sh)	472	1.9	0.51	462, 493
Ir5b	232 (47.6), 263 (44.0), 378 (5.9)	469, 488(sh)	475	1.8	0.69	467, 496
Ir6a	256 (51.2), 375 (4.5)	474, 499	474	1.9	0.63	469, 499
Ir6b	254 (42.0), 376 (4.8)	473, 498	475	1.8	0.61	470, 502
Ir7a	255(43.3), 291(24.2), 380(3.9)	471, 498	474	1.9	0.28	465, 496
Ir7b	256 (32.9), 377 (3.7)	471, 497	476	1.7	0.33	471, 501
Ir8a	252 (39.1), 373 (2.7)	470, 499	472	1.7	0.11	468, 498
Ir8b	251 (37.1), 372 (4.8)	455, 479	457, 481	1.9	0.32	451, 463, 482

[a] Measured in CH_2Cl_2 solutions (~5×10^{-6} M). [b] Measured in deaerated solutions (~5×10^{-5} M), λ_{ex} = 380 nm, sh = shoulder. [c] Take *fac*-Ir(ppy)$_3$ in CH_2Cl_2 as reference (~5×10^{-5} M, Φ_{PL} = 0.40).

tions between 230 and 280 nm which can be assigned to spin allowed $^1\pi-\pi^*$ ligand centered (LC) transitions involving the dfppy and NHCs. The moderate absorption bands between 300−400 nm are corresponding to the spin allowed metal to ligand charge-transfer (^{1}MLCT) transitions, partially overlapped by the broad LC absorptions. The weak absorption tails after 400 nm can be assigned as the theoretically forbidden ^{3}MLCT transitions, caused by the large spin orbital coupling (SOC) that was introduced by iridium center. No distinct difference is observed in absorption profiles for all the complexes, indicating the similar electronic and vibrational structures of the ground states (S_0) and the first excited states (S_1). The detailed assignments of the absorption spectra are clarified and confirmed by the TD-DFT calculations (Supporting Information, Figure S3, Table S5) for completeness. All the complexes own alike $S_0 \rightarrow S_n$ transitions in the same range of wavelength with similar oscillator strength. This confirms the resemblance of UV−vis absorption spectra of these complexes.

For phosphorescent emitters used in OLEDs, significant mixing of the lowest triplet and higher-lying singlet excited states caused by efficient SOC is in favor of high phosphorescent quantum efficiency. Meanwhile, strong SOC effect can drastically shorten the emission decay time and depress the triplet−triplet annihilation. The emission spectra in CH_2Cl_2 exhibit maximum peaks in the range of 455−485 nm generated from the electronic 0−0 transition between the lowest triplet excited state to the ground state, making them blue or greenish-blue phosphors. The emission at lower energy range (~490 nm) might stem from overlapping vibrational satellites.[32] All the emission spectra are obviously less structured than that of FIr6[13] but are much better resolved than that of *fac*-Ir(ppy)$_3$ (ppy = 2-phenylpyridinate) in similar conditions.[33] This indicates that the MLCT characters involved in the emitting T_1 states of different complexes are various, but significant, since a dominant MLCT character in T_1 usually leads to large inhomogeneity and low-energy lying metal—ligand vibrational satellites, smearing out the spectrum below the electronic original emission.[34]

Obviously, in Figure 5, both at room temperature and 77 K, the emission spectra of **Ir2a**/**Ir2b** are less structured without shoulder peaks compared with the others. These differences are generated from the nature of these two complexes determined by their chemical structures. To our knowledge, the iridium phosphors with pure MLCT emission states will present a broad and structureless emission, such as *fac*-Ir(ppy)$_3$, which has a broad emission even at very low temperature. **Ir2a**/**Ir2b** present a broad emission at 77 K demonstrating that the emission states of these two complexes are mainly dominated by MLCT characters. The other complexes, namely, **Ir1a**/**Ir1b** and **Ir3a**-**Ir8a**/**Ir3b**-**Ir8b**, are slightly structured at room temperature and highly structured at 77 K. These again demonstrate that their emission states are hybrid states with major ^{3}MLCT and minor ^{3}ILCT characters.

Although the theoretical calculation results indicate that the HOMOs and LUMOs are further stabilized and the $\Delta E_{\mathrm{HOMO-LUMO}}$ are broadened, when the phenyl moiety is replaced by pyridyl or pyrimidyl in **Ir6a**/**Ir6b**, **Ir7a**/**Ir7b**, and **Ir8a**, their emission peaks are shown at ~470 nm without obvious hypsochromic shifts. It may result from the stabilization of the emissive T_1 excited states simultaneously. Although broad $\Delta E_{\mathrm{HOMO-LUMO}}$ are favorable to hypsochromic shifts, the excited states are not necessarily arising from the HOMO to LUMO excitations. However, it is noteworthy that **Ir8b** has a significant hypsochromic shift and the first emission peak is 457 nm, suggesting that this emission may come from a higher-lying emissive state in energy. This hypothesis can be proved by its emission spectrum at 77 K, in which the first emission peak at ambient temperature splits into two peaks of 451 and 463 nm together with another peak at 482 nm. The latter two peaks are comparable with those in other complexes, and the first peak is generated from a higher-lying hybrid emissive state. Most of the Ir(III) phosphors have satisfying photoluminescence quantum efficiencies up to 0.73.

To demonstrate that the Ir(III) complexes are promising emitters for OLEDs, we measured the photoluminescent spectra of all the blue and greenish-blue complexes doped in widely used host material of mCP with the concentration of 10 wt %, and the amorphous films were excited by the maximum exciting wavelength of 320 nm for pure mCP (Supporting Information, Figure S4). From this figure, we found the doped amorphous films present the emission peaks of the iridium complexes, and the emission of the mCP at 361 nm cannot be observed. The results demonstrate that the energy transfer from the host material to the dopants is complete. Also, we found that **Ir5b** has the highest photoluminescent intensity and efficiency among all the spectra recorded at the same conditions. These results make it convincing that the iridium phosphors reported in this manuscript are suitable for OLEDs, and **Ir5b** is a promising emitter.

Different Color Emitters with Carbene Ligand. Because the NHCs are σ-donating ligands with high triplet energy levels, most neutral and cationic iridium complexes are blue phosphorescent emitters. To demonstrate that they are versatile second cyclometalated ligands for neutral Ir(III) phosphors, **L5a** was chosen to prepare another five complexes with different C^N cyclometalated ligands, namely, 2′,6′-difluoro-2,3′-bipyridine (dfpypy), 2-(3-(trifluoromethyl)phenyl) pyridine (3-tfmppy), 2-(4-(trifluoromethyl)phenyl)pyridine (4-tfmppy), 2-(dibenzo[b,d]thiophen-4-yl) pyridine (dbthppy), and 1-(4-(trifluoromethyl)phenyl) isoquinoline (4-tfmpiq), to cover the emission range from blue to red. The chemical structures of these complexes and reported complexes with corresponding C^N ligands and conventional ancillary ligands (e.g., acac, pic, and tpip (tetraphenylimidodiphosphinate)) for references are presented in Scheme 2. The single-crystal structures of **Ir9** and **Ir11** were depicted in Figure 6. The UV−vis absorption spectra and photoluminescent spectra of these complexes were shown in Figure 7. Their photophysical data were collected in Table 2. As shown in Figure 7, all the complexes own intense absorption bands in high-energy range assigned to LC charge transfer and low-energy absorption bands generated by MLCT. The emission peaks of these complexes are in a wide range from 464 to 603 nm, and all the emissions are structureless, indicating the MLCT character of their emission states.

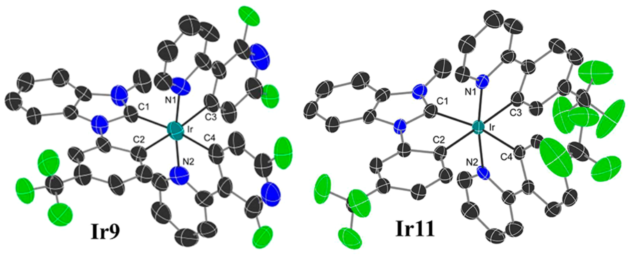

Figure 6. Perspective diagrams of X-ray crystal structures of **Ir9** and **Ir11**. (Thermal ellipsoids shown at 40% probability level; H atoms and solvent molecules are omitted for clarity.) Labels are added on the atoms bonded to the iridium center.

According to the TD-DFT calculations, the lowest allowed transitions generate from a combination of HOMO−1 ($d_{\mathrm{Ir}}+\pi_{\mathrm{dfpypy}}$) → LUMO ($\pi^*_{\mathrm{dfpypy}}$) and HOMO ($d_{\mathrm{Ir}}+\pi_{\mathrm{L5a}}$) → LUMO for **Ir9** and from only HOMO ($d_{\mathrm{Ir}}+\pi_{\text{first cyclometalated ligand}}$) → LUMO ($\pi^*_{\text{first cyclometalated ligand}}$) for **Ir5a** and **Ir10**-**Ir13**. The $S_0 \rightarrow S_1$ transition absorption peaks locate at 285.6, 304.4, 312.2, 321.5, 334.3, and 364.7 nm for **Ir9**, **Ir5a**, **Ir10**, **Ir11**, **Ir12**, and **Ir13**, respectively. The result correspond to the emission sequence.

To evaluate the effects exerted by NHCs on the photophysical properties, the photoluminescence of these complexes was compared with some reported Ir(III) emitters. Because of the stronger ligand field induced by carbene than by acac and tpip, the separation of the iridium *d* orbitals is larger. Consequently, in the comparisons of **Ir10**/**Ir10-r**, **Ir11**/**Ir11-r**, and **Ir13**/**Ir13-r**, the emission peaks of the formers are about 30 nm shorter than the latter references. Moreover, the quantum yields of the synthesized couples are comparable or even better than reported ones. Meanwhile, we found that the emission peak of **Ir5a** is 5 nm shorter than that of FIrpic, suggesting that **L5a** has comparable ligand field strength to that of pic. However, in the case of **Ir9**/**Ir9-r**, since the T_1 energy

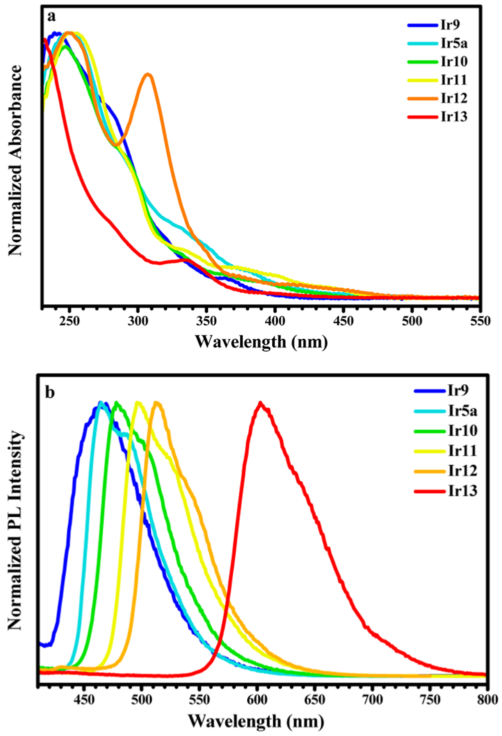

Figure 7. Normalized UV−vis absorption (a) and emission spectra (b) in CH_2Cl_2 at ambient temperature for **Ir9**, **Ir5a**, **Ir10**, **Ir11**, **Ir12**, and **Ir13**.

Table 2. Photophysical Properties of the Synthesized and Reported Iridium Complexes with Relevant C^N Ligands

complex	absorption[a] λ_{abs} (ε) (nm ($\times 10^{-3}$ L mol^{-1} cm^{-1}))	photoluminescence[a] λ_{max} (nm)	τ (μs)	Φ_{PL}
Ir9	239 (50.8), 278 (36.6)sh, 363 (3.9)	464	2.1	0.09
Ir9-r[38]	246 (42.0), 377 (4.3), 443 (0.4)	457/459	1.8	0.67
Ir5a	249 (57.2), 285 (31.8), 377 (6.4)	465	1.9	0.51
FIrpic[39]	255 (43.16), 282 (26.0)sh, 377 (5.3), 455 (0.4)	470	1.9	0.83
Ir10	247 (51.3), 285 (30.7)sh, 331 (9.1), 390 (3.4)	478	1.9	0.25
Ir10-r[11c]	268 (39.3), 293 (24.2), 342 (7.1), 454 (2.3)	502	2.1	0.07
Ir11	252 (52.1), 289 (28.4)sh, 329 (9.8), 372 (6.2), 433 (2.4)	496	1.7	0.32
Ir11-r[11c]	270 (55.4), 359 (10.2), 408 (4.1), 458 (3.4)	524	1.9	0.23
Ir12[b]	249 (72.5), 307 (61.1), 413 (3.6)	512	1.8	0.30
Ir13	230 (82.7), 277 (24.7)sh, 334 (11.8)	603	2.1	0.62
Ir13-r[40]	309, 343, 397 (5.2), 468 (4.5)	631	*c*	0.31

[a]Recorded in CH_2Cl_2 at ambient temperature. [b]There is no reported analogous iridium phosphor with dbthppy cyclometalated ligand. [c]Not reported.

level of the dfpypy is very high,[6] the ligand field effect generated by the carbene ligand is limited, and the emission states of them are both dominated by the MLCT character. Therefore, no obvious hypsochromatic shift was observed.

Electroluminescence Performance. Because the complex **Ir5b** has the similar emission to that of **Ir5a** and even higher efficiency in both solution and amorphous film, the OLED with the structure of ITO/TAPC (1,1-bis(4-(di-*p*-tolylamino)-phenyl)cyclohexane, 40 nm)/**Ir5b** (9 wt %): mCP (20 nm)/TmPyPB (1,3,5-tri(*m*-pyrid-3-yl-phenyl)benzene, 40 nm)/LiF (1 nm)/Al (100 nm) was fabricated with optimized dopant concentration of 9 wt % as an example to evaluate the electroluminescence (EL) performances of our carbene-based emitters. The energy diagrams of the device, as well as the molecular structures of the materials used, are shown in Figure 8. Obviously, the HOMO/LUMO levels of the **Ir5b** complex are all within that of host material mCP. The LUMO (−3.11 eV) of the **Ir5b** complex is even lower than that of the electron-transport material TmPyPB. So, a good carrier trapping is expected in the device, which is the dominant EL mechanism. Furthermore, holes and electrons will be well-confined within the doped light-emitting layer.

The EL spectrum current density (J) and luminance (L) versus voltage (V), luminance versus current efficiency (η_c) characteristics of the device are also shown in Figure 8. The device emits blue light with the EL emission peak at 470 nm. The emission spectra are almost invariant of the current density and are very close to the PL spectrum of the **Ir5b** complex in CH_2Cl_2 solution, indicating that the EL emission of the device originates from the triplet excited states of the phosphor. The turn-on voltage ($V_{turn-on}$) of this device is 3.4 V, and the maximum η_c and external quantum efficiency (η_{ext}) are 37.83 cd A^{-1} and 10.3%, respectively. The maximum luminance (L_{max}) of 8709 cd m^{-2} can be obtained at 11.7 V. The performances are even comparable to that of the devices using the famous sky blue emitter FIrpic as the emitter.[35]

We believe the relative good device performances are due to the low LUMO energy level and good electron mobility of the **Ir5b** complex because the dopant acts as the hole and electron traps to retard the motion of both types of carriers. The low LUMO level of the dopant is particularly important for the reason that the hole mobility of the TAPC is higher than the electron mobility of the TmPyPB,[36] and the excitons accumulation is expected in hole-blocking layer near the interface of emitting layer (Ir complex: mCP)/TmPyPB due to the high energy barrier between TmPyPB and mCP.[37] The accumulation of excitons is expected to cause the serious triplet−triplet annihilation (TTA) and triplet−polaron annihilation (TPA) of the Ir(III) complexes, and low efficiency consequently. In our case, the LUMO level of the dopant is lower than that of the mCP, and the TmPyPB will benefit the electron-transport properties. The good electron mobility of the phosphorescent emitter would facilitate the injection and transport of electrons, which broadens the recombination zone, balances the distribution of holes and electrons, and reduces leakage current, particularly for the high doping concentration, leading to the suppressed TTA, TPA effects,[41] and improved recombination probability and device efficiency.

But the device showed serious efficiency roll-off at higher brigtness due to two posibilities. One is the stability problem of the complexes. But most of the iridium complexes with F/CF_3 units can be sublimated to form crystals. Another reason is the population of the excited state of the blue emitter. The long lifetime of the blue Ir(III) complexes will cause serious triplet−triplet annihilation (especially in high dopant concentration) and triplet−polaron annihilation (especially at high current density). An ∼2 μs lifetime for our complexes perhaps is a problem. In our future work we will try to synthesize the iridium phosphors with reduced lifetime based on cyclometalated NHCs.

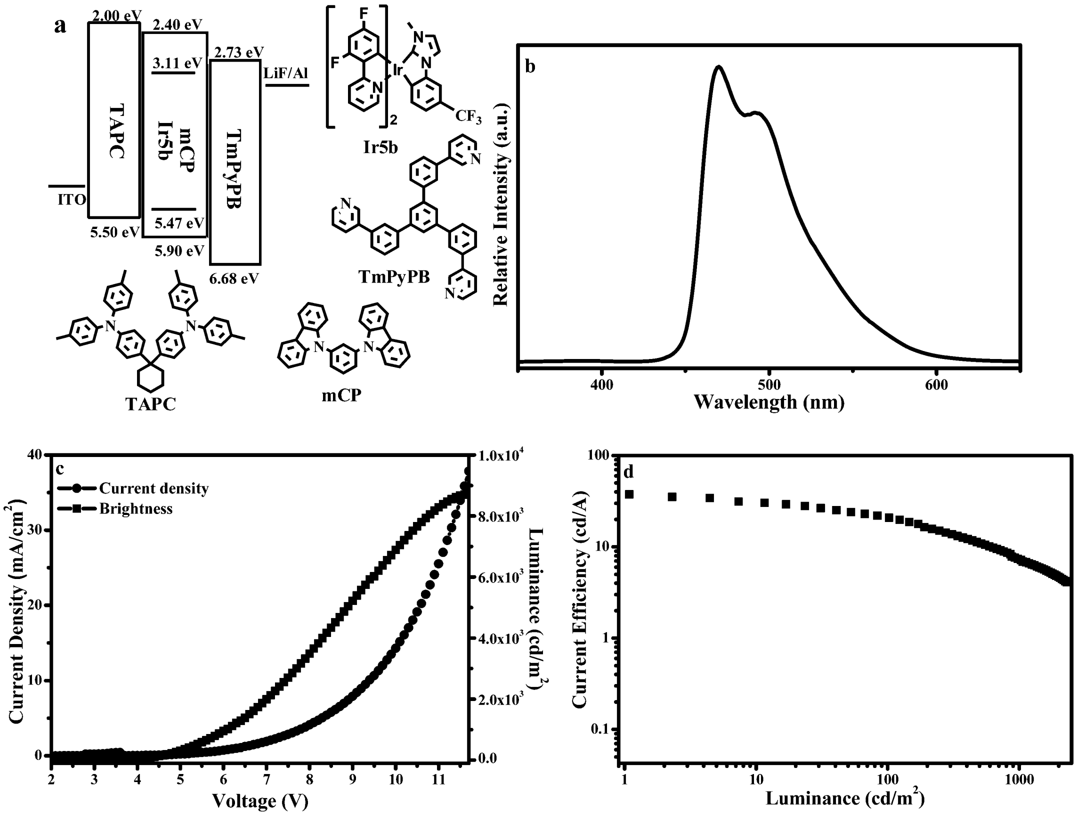

Figure 8. (a) Energy level diagrams of HOMO and LUMO levels (relative to vacuum level) and molecular structures for materials investigated; (b) EL spectrum; (c) J–V–L curves; (d) η_c–L curve.

4. CONCLUSION

In summary, by using monoanionic NHCs as the second cyclometalated ligands, a series of iridium complexes of the new type, (C^N)$_2$Ir(NHC), have been successfully synthesized. They are good models for investigating the NHC effect on the emitting properties. By modifying the NHCs, the HOMO composition and energy could be controlled. Consequently, the emission peaks of 16 blue or greenish-blue emitters were tunable within tens of nanometers at ~470 nm. Additionally, with the use of different C^N ligands, another five emitters nearly covering all the visible wavelength range from 464 to 603 nm were also prepared. More importantly, the OLED with **Ir5b** exhibits good performances with a maximum η_c of 37.83 cd A^{-1}, an η_{ext} of 10.3%, and an L_{max} of 8709 cd m^{-2}. The NHC is a kind of versatile and ideal ligand for neutral Ir(III) phosphorescent complexes with different colors. Our study suggests that the Ir(III) complexes with NHCs as the second cyclometalated ligands have several advantages: (1) easy synthetic chemical accessibility; (2) NHCs have strong ligand field, which can tune the emission in a wide range; (3) the devices using (C^N)$_2$Ir(NHC) as the emitter show good performances. Although most of the materials reported are sky-blue emitters, we have demonstrated that the replacement of ancillary ligands with NHCs can indeed adjust the emission peak wavelength. Further work on new materials and OLEDs with second cyclometalated NHCs aiming at true blue and full color, high efficiency, and low-efficiency roll off, is underway in our laboratory.

■ ASSOCIATED CONTENT

Ⓢ Supporting Information

X-ray crystallographic data of the complexes in CIF format, tabulated crystal information and structure data, cyclic voltammograms, theoretical calculation results and emission spectra of **Ir1a/1b** to **Ir8a/8b** in mCP thin film, and the decay curves of the complexes. This material is available free of charge via the Internet at http://pubs.acs.org.

■ AUTHOR INFORMATION

Corresponding Author

*E-mail: yxzheng@nju.edu.cn.

Notes

The authors declare no competing financial interest.

■ ACKNOWLEDGMENTS

This work was supported by the National Natural Science Foundation of China (21371093, 21201161, 91433113), the Major State Basic Research Development Program (2011CB808704, 2013CB922101, 2014CB643802), and the Natural Science Foundation of Jiangsu Province (BK20130054).

■ REFERENCES

(1) (a) Adachi, C.; Baldo, M. A.; Forrest, S. R.; Thompson, M. E. *Appl. Phys. Lett.* **2000**, *77*, 904–906. (b) Lamansky, S.; Djurovich, P.; Murphy, D.; Abdel-Razzaq, F.; Lee, H. E.; Adachi, C.; Burrows, P. E.; Forrest, S. R.; Thompson, M. E. *J. Am. Chem. Soc.* **2001**, *123*, 4304–4312. (c) Muller, C. D.; Falcou, A.; Reckefuss, N.; Rojahn, M.; Wiederhirn, V.; Rudati, P.; Frohne, H.; Nuyken, O.; Becker, H.; Meerholz, K. *Nature* **2003**, *421*, 829–833. (d) Holder, E.; Langeveld,

B. M. W.; Schubert, U. S. *Adv. Mater.* **2005**, *17*, 1109−1121. (e) Wong, W. Y.; Ho, C. L. *Coord. Chem. Rev.* **2009**, *253*, 1709−1758. (f) Xiao, L. X.; Chen, Z. J.; Qu, B.; Luo, J. X.; Kong, S.; Gong, Q. H.; Kido, J. J. *Adv. Mater.* **2011**, *23*, 926−952. (g) Costa, R. D.; Orti, E.; Bolink, H. J.; Monti, F.; Accorsi, G.; Armaroli, N. *Angew. Chem., Int. Ed.* **2012**, *51*, 8178−8211. (h) Lee, S.; Kim, S. O.; Shin, H.; Yun, H. J.; Yang, K.; Kwon, S. K.; Kim, J. J.; Kim, Y. H. *J. Am. Chem. Soc.* **2013**, *135*, 14321−14328.

(2) (a) You, Y. M.; Park, S. Y. *J. Am. Chem. Soc.* **2005**, *127*, 12438−12439. (b) Zhou, G. J.; Ho, C. L.; Wong, W. Y.; Wang, Q.; Ma, D. G.; Wang, L. X.; Lin, Z. Y.; Marder, T. B.; Beeby, A. *Adv. Funct. Mater.* **2008**, *18*, 499−511. (c) Yang, X. L.; Sun, N.; Dang, J. S.; Huang, Z.; Yao, C. L.; Xu, X. B.; Ho, C. L.; Zhou, G. J.; Ma, D. G.; Zhao, X.; Wong, W. Y. *J. Mater. Chem. C* **2013**, *1*, 3317−3326. (d) Baranoff, E.; Bolink, H. J.; Constable, E. C.; Delgado, M.; Haussinger, D.; Housecroft, C. E.; Nazeeruddin, M. K.; Neuburger, M.; Orti, E.; Schneider, G. E.; Tordera, D.; Walliser, R. M.; Zampese, J. A. *Dalton Trans.* **2013**, *42*, 1073−1087.

(3) (a) Liu, S. J.; Zhao, Q.; Deng, Y.; Xia, Y. J.; Lin, J.; Fan, Q. L.; Wang, L. H.; Huang, W. *J. Phys. Chem. C* **2007**, *111*, 1166−1175. (b) Zhou, G. J.; Wong, W. Y.; Yao, B.; Xie, Z. Y.; Wang, L. X. *Angew. Chem., Int. Ed.* **2007**, *46*, 1149−1151. (c) Gather, M. C.; Kohnen, A.; Meerholz, K. *Adv. Mater.* **2011**, *23*, 233−248. (d) Zhuang, J. Y.; Li, W. F.; Su, W. M.; Liu, Y.; Shen, Q.; Liao, L. S.; Zhou, M. *Org. Electron.* **2013**, *14*, 2596−2601. (e) Sasabe, H.; Nakanishi, H.; Watanabe, Y.; Yano, S.; Hirasawa, M.; Pu, Y. J.; Kido, J. *Adv. Funct. Mater.* **2013**, *23*, 5550−5555. (f) Wang, J.; Liu, J.; Huang, S. J.; Wu, X. K.; Shi, X. D.; Chen, C. P.; Ye, Z. C.; Lu, J. G.; Su, Y. K.; He, G. F.; Zheng, Y. X. *Org. Electron.* **2013**, *14*, 2854−2858. (g) Fan, C.; Miao, J. S.; Jiang, B.; Yang, C. L.; Wu, H. B.; Qin, J. G.; Cao, Y. *Org. Electron.* **2013**, *14*, 3392−3398.

(4) Chen, Z. Q.; Bian, Z. Q.; Huang, C. H. *Adv. Mater.* **2010**, *22*, 1534−1539.

(5) Chen, L. Q.; You, H.; Yang, C. L.; Ma, D. G.; Qin, J. G. *Chem. Commun.* **2007**, 1352−1354.

(6) Lee, S. J.; Park, K. M.; Yang, K.; Kang, Y. *Inorg. Chem.* **2009**, *48*, 1030−1037.

(7) Wu, L. L.; Yang, C. H.; Sun, I. W.; Chu, S. Y.; Kao, P. C.; Huang, H. H. *Organometallics* **2007**, *26*, 2017−2023.

(8) Kessler, F.; Watanabe, Y.; Sasabe, H.; Katagiri, H.; Nazeeruddin, M. K.; Graetzel, M.; Kido, J. *J. Mater. Chem. C* **2013**, *1*, 1070−1075.

(9) (a) Tamayo, A. B.; Alleyne, B. D.; Djurovich, P. I.; Lamansky, S.; Tsyba, I.; Ho, N. N.; Bau, R.; Thompson, M. E. *J. Am. Chem. Soc.* **2003**, *125*, 7377−7387. (b) Lo, S. C.; Shipley, C. P.; Bera, R. N.; Harding, R. E.; Cowley, A. R.; Burn, P. L.; Samuel, I. D. W. *Chem. Mater.* **2006**, *18*, 5119−5129. (c) He, L.; Qiao, J.; Duan, L.; Dong, G. F.; Zhang, D. Q.; Wang, L. D.; Qiu, Y. *Adv. Funct. Mater.* **2009**, *19*, 2950−2960.

(10) Yang, C. H.; Mauro, M.; Polo, F.; Watanabe, S.; Muenster, I.; Froehlich, R.; Cola, L. D. *Chem. Mater.* **2012**, *24*, 3684−3695.

(11) (a) Zhu, Y. C.; Zhou, L.; Li, H. Y.; Xu, Q. L.; Teng, M. Y.; Zheng, Y. X.; Zuo, J. L.; Zhang, H. J.; You, X. Z. *Adv. Mater.* **2011**, *23*, 4041−4046. (b) Li, H. Y.; Zhou, L.; Teng, M. Y.; Xu, Q. L.; Lin, C.; Zheng, Y. X.; Zuo, J. L.; Zhang, H. J.; You, X. Z. *J. Mater. Chem. C* **2013**, *1*, 560−565. (c) Xu, Q. L.; Wang, C. C.; Li, T. Y.; Teng, M. Y.; Zhang, S.; Jing, Y. M.; Yang, X.; Li, W. N.; Lin, C.; Zheng, Y. X.; Zuo, J. L.; You, X. Z. *Inorg. Chem.* **2013**, *52*, 4916−4925. (d) Wang, C. C.; Jing, Y. M.; Li, T. Y.; Xu, Q. L.; Zhang, S.; Li, W. N.; Zheng, Y. X.; Zuo, J. L.; You, X. Z.; Wang, X. Q. *Eur. J. Inorg. Chem.* **2013**, 5683−5693. (e) Li, T. Y.; Liang, X.; Wu, C.; Xue, L. S.; Xu, Q. L.; Zhang, S.; Liu, X.; Zheng, Y. X.; Wang, X.-Q. *J. Organomet. Chem.* **2014**, *755*, 110−119. (f) Li, H. Y.; Li, T. Y.; Teng, M. Y.; Xu, Q. L.; Zhang, S.; Jin, Y. M.; Liu, X.; Zheng, Y. X.; Zuo, J. L. *J. Mater. Chem. C* **2014**, *2*, 1116−1124.

(12) (a) Adachi, C.; Kwong, R. C.; Djurovich, P.; Adamovich, V.; Baldo, M. A.; Thompson, M. E.; Forrest, S. R. *Appl. Phys. Lett.* **2001**, *79*, 2082−2084. (b) Holmes, R. J.; Forrest, S. R.; Tung, Y. J.; Kwong, R. C.; Brown, J. J.; Garon, S.; Thompson, M. E. *Appl. Phys. Lett.* **2003**, *82*, 2422−2424.

(13) Holmes, R. J.; D'Andrade, B. W.; Forrest, S. R.; Ren, X.; Li, J.; Thompson, M. E. *Appl. Phys. Lett.* **2003**, *83*, 3818−3820.

(14) Sajoto, T.; Djurovich, P. I.; Tamayo, A.; Yousufuddin, M.; Bau, R.; Thompson, M. E.; Holmes, R. J.; Forrest, S. R. *Inorg. Chem.* **2005**, *44*, 7992−8003.

(15) Chang, C. F.; Cheng, Y. M.; Chi, Y.; Chiu, Y. C.; Lin, C. C.; Lee, G. H.; Chou, P. T.; Chen, C. C.; Chang, C. H.; Wu, C. C. *Angew. Chem., Int. Ed.* **2008**, *47*, 4542−4545.

(16) (a) Hsieh, C. H.; Wu, F. I.; Fan, C. H.; Huang, M. J.; Lu, K. Y.; Chou, P. Y.; Yang, Y. H. O.; Wu, S. H.; Chen, I. C.; Chou, S. H.; Wong, K. T.; Cheng, C. H. *Chem.—Eur. J.* **2011**, *17*, 9180−9187. (b) Lu, K. Y.; Chou, H. H.; Hsieh, C. H.; Yang, Y. H. O.; Tsai, H. R.; Tsai, H. Y.; Hsu, L. C.; Chen, C. Y.; Chen, I. C.; Cheng, C. H. *Adv. Mater.* **2011**, *23*, 4933−4937.

(17) (a) Kessler, F.; Costa, R. D.; Di Censo, D.; Scopelliti, R.; Orti, E.; Bolink, H. J.; Meier, S.; Sarfert, W.; Gratzel, M.; Nazeeruddin, M. K.; Baranoff, E. *Dalton Trans.* **2012**, *41*, 180−191. (b) Meier, S. B.; Sarfert, W.; Junquera-Hernandez, J. M.; Delgado, M.; Tordera, D.; Orti, E.; Bolink, H. J.; Kessler, F.; Scopelliti, R.; Gratzel, M.; Nazeeruddin, M. K.; Baranoff, E. *J. Mater. Chem. C* **2013**, *1*, 58−68.

(18) Chien, C. H.; Fujita, S.; Yamoto, S.; Hara, T.; Yamagata, T.; Watanabe, M.; Mashima, K. *Dalton Trans.* **2008**, 916−923.

(19) King, K. A.; Spellane, P. J.; Watts, R. J. *J. Am. Chem. Soc.* **1985**, *107*, 1431−1432.

(20) *SAINT-Plus,* version 6.02; Bruker Analytical X-ray Systems: Madison, WI, 1999.

(21) Sheldrick, G. M. *SADABS,* An empirical absorption correction program; Bruker Analytical X-ray Systems: Madison, WI, 1996.

(22) Sheldrick, G. M. *SHELXTL-97;* Universität of Göttingen: Göttingen, Germany, 1997.

(23) Frisch, M. J.; Trucks, G. W.; Schlegel, H. B.; Scuseria, G. E.; Robb, M. A.; Cheeseman, J. R.; Scalmani, G.; Barone, V.; Mennucci, B.; Petersson, G. A.; Nakatsuji, H.; Caricato, M.; Li, X.; Hratchian, H. P.; Izmaylov, A. F.; Bloino., J.; Zheng, G.; Sonnenberg, J. L.; Hada, M.; Ehara, M.; Toyota, K.; Fukuda, R.; Hasegawa, J.; Ishida, M.; Nakajima, T.; Honda, Y.; Kitao, O.; Nakai, H.; Vreven, T.; Montgomery, J. A., Jr.; Peralta, J. E.; Ogliaro, F.; Bearpark, M.; Heyd, J. J.; Brothers, E.; Kudin, K. N.; Staroverov, V. N.; Kobayashi, R.; Normand, J.; Raghavachari, K.; Rendell, A.; Burant, J. C.; Iyengar, S. S.; Tomasi, J.; Cossi, M.; Rega, N.; Millam, J. M.; Klene, M.; Knox, J. E.; Cross, J. B.; Bakken, V.; Adamo, C.; Jaramillo, J.; Gomperts, R.; Stratmann, R. E.; Yazyev, O.; Austin, A. J.; Cammi, R.; Pomelli, C.; Ochterski, J. W.; Martin, R. L.; Morokuma, K.; Zakrzewski, V. G.; Voth, G. A.; Salvador, P.; Dannenberg, J. J.; Dapprich, S.; Daniels, A. D.; Farkas, O.; Foresman, J. B.; Ortiz, J. V.; Cioslowski, J.; Fox, D. J. *Gaussian 09*, Revision A.01; Gaussian, Inc.: Wallingford, CT, 2009.

(24) (a) Lee, C. T.; Yang, W. T.; Parr, R. G. *Phys. Rev. B* **1988**, *37*, 785−789. (b) Becke, A. D. *J. Chem. Phys.* **1993**, *98*, 5648−5652. (c) Hay, P. J. *J. Phys. Chem. A* **2002**, *106*, 1634−1641.

(25) Hay, P. J.; Wadt, W. R. *J. Chem. Phys.* **1985**, *82*, 299−310.

(26) Francl, M. M.; Pietro, W. J.; Hehre, W. J.; Binkley, J. S.; Gordon, M. S.; Defrees, D. J.; Pople, J. A. *J. Chem. Phys.* **1982**, *77*, 3654−3665.

(27) Barone, V.; Cossi, M. *J. Phys. Chem. A* **1998**, *102*, 1995−2001.

(28) Zhao, Y.; Truhlar, D. G. *J. Phys. Chem. A* **2006**, *110*, 5121−5129.

(29) Sprouse, S.; King, K. A.; Spellane, P. J.; Watts, R. J. *J. Am. Chem. Soc.* **1984**, *106*, 6647−6653.

(30) Monti, F.; Kessler, F.; Delgado, M.; Frey, J.; Bazzanini, F.; Accorsi, G.; Armaroli, N.; Bolink, H. J.; Orti, E.; Scopelliti, R.; Nazeeruddin, M. K.; Baranoff, E. *Inorg. Chem.* **2013**, *52*, 10292−10305.

(31) Stringer, B. D.; Quan, L. M.; Barnard, P. J.; Wilson, D. J. D.; Hogan, C. F. *Organometallics* **2014**, *33*, 4860−4872.

(32) Rausch, A. F.; Thompson, M. E.; Yersin, H. *Inorg. Chem.* **2009**, *48*, 1928−1937.

(33) (a) Finkenzeller, W. J.; Yersin, H. *Chem. Phys. Lett.* **2003**, *377*, 299−305. (b) Hofbeck, T.; Yersin, H. *Inorg. Chem.* **2010**, *49*, 9290−9299.

(34) (a) Wilde, A. P.; Watts, R. J. *J. Phys. Chem.* **1991**, *95*, 622−629. (b) Colombo, M. G.; Brunold, T. C.; Riedener, T.; Gudel, H. U.; Fortsch, M.; Burgi, H. B. *Inorg. Chem.* **1994**, *33*, 545−550.

(35) (a) Shih, P. I.; Chien, C. H.; Chuang, C. Y.; Shu, C. F.; Yang, C. H.; Chen, J. H.; Chi, Y. *J. Mater. Chem.* **2007**, *17*, 1692−1698. (b) Hsu, F. M.; Chien, C. H.; Shu, C. F.; Lai, C. H.; Hsieh, C. C.; Wang, K. W.; Chou, P. T. *Adv. Funct. Mater.* **2009**, *19*, 2834−2843. (c) Hsu, F. M.; Chien, C. H.; Shih, P. I.; Shu, C. F. *Chem. Mater.* **2009**, *21*, 1017−1022. (d) Rothmann, M. M.; Haneder, S.; Da Como, E.; Lennartz, C.; Schildknecht, C.; Strohriegl, P. *Chem. Mater.* **2010**, *22*, 2403−2410. (e) Cui, L. S.; Liu, Y.; Yuan, X. D.; Li, Q.; Jiang, Z. Q.; Liao, L. S. *J. Mater. Chem. C* **2013**, *1*, 8177−8185. (f) Han, C. M.; Zhao, F. C.; Zhang, Z.; Zhu, L. P.; Xu, H.; Li, J.; Ma, D. G.; Yan, P. F. *Chem. Mater.* **2013**, *25*, 4966−4976. (g) Wagner, D.; Hoffmann, S. T.; Heinemeyer, U.; Munster, I.; Kohler, A.; Strohriegl, P. *Chem. Mater.* **2013**, *25*, 3758−3765. (h) Deng, L. J.; Li, J. Y.; Wang, G. X.; Wu, L. Z. *J. Mater. Chem. C* **2013**, *1*, 8140−8145.

(36) Fong, H. H.; Lun, K. C.; So, S. K. *Chem. Phys. Lett.* **2002**, *353*, 407−413.

(37) Parker, I. D. *J. Appl. Phys.* **1994**, *75*, 1656−1666.

(38) Kang, Y.; Chang, Y. L.; Lu, J. S.; Ko, S. B.; Rao, Y. L.; Varlan, M.; Lu, Z. H.; Wang, S. N. *J. Mater. Chem. C* **2013**, *1*, 441−450.

(39) Rausch, A. F.; Thompson, M. E.; Yersin, H. *J. Phys. Chem. A* **2009**, *113*, 5927−5932.

(40) Fang, K. H.; Wu, L. L.; Huang, Y. T.; Yang, C. H.; Sun, I. W. *Inorg. Chim. Acta* **2006**, *359*, 441−450.

(41) (a) Kalinowski, J.; Stampor, W.; Mezyk, J.; Cocchi, M.; Virgili, D.; Fattori, V.; Di Marco, P. *Phys. Rev. B* **2002**, *66*, 235321. (b) Jeon, W. S.; Park, T. J.; Kim, S. Y.; Pode, R.; Jang, J.; Kwon, J. H. *Appl. Phys. Lett.* **2008**, *93*, 063303.